

TEMPORAL CORRELATION BETWEEN OUTBURSTS AND FRAGMENTATION EVENTS OF COMET 168P/HERGENROTHER

ZDENEK SEKANINA

Jet Propulsion Laboratory, California Institute of Technology
4800 Oak Grove Drive, Pasadena, CA 91109

Version August 21, 2018

ABSTRACT

Outbursts are known to begin with a sudden appearance and steep brightening of a “stellar nucleus” — an unresolved image of a plume of material on its way from the comet’s surface and an initial stage of an expanding halo of ejecta. Since the brightness of this feature is routinely reported, together with astrometry, by most comet observers as the “nuclear magnitude,” it is straightforward to determine the onset time, a fundamental parameter of any outburst, by inspecting the chronological lists of such observations for a major jump in the nuclear brightness. Although it is inadmissible to mix nuclear magnitudes by different observers without first carefully examining their compatibility, the time constraints obtained from data sets reported by different observers can readily be combined. The intersection of these sets provides the tightest possible constraint on the outburst’s onset time. Applied to comet 168P/Hergenrother during its 2012 return to perihelion, three outbursts were detected and their timing determined with good to excellent accuracy. Six fragmentation events experienced by the comet are shown to have occurred in the same period of time as the outbursts. Three companions are likely to have broken off from the primary in the first outburst, two companions in the second outburst, and one companion in the last outburst. All companions were short-lived, belonging to the class of excessively brittle fragments. Yet, the results suggest that most of the mass lost in the first outburst remained relatively intact during the liftoff, while the opposite was the case in the last outburst.

Subject headings: comets-nucleus, comets-coma, comets-dust

1. INTRODUCTION

Two classes of phenomena that always attract much attention of comet observers are outbursts and nucleus’ fragmentation. Not unexpectedly, they fairly often — though not always — correlate, but sometimes it is not easy to provide convincing evidence for this correlation. The solution is particularly difficult when there are several outbursts and/or more than one companion to the primary nucleus in a relatively short period of time.

The major observational difference between outbursts and fragmentation (or splitting) events is that outbursts are detected practically as they happen, subject only to (i) the light time, (ii) a large enough amplitude for the observer to notice it as a jump in brightness, and (iii) his opportunity to observe the comet at the critical time. By contrast, sizable fragments of the nucleus, with separation velocities in the submeter- to meter-per-second range, do not get resolved from the parent nucleus until at least a few weeks, but more often a month or longer after splitting. Besides, nucleus’ fragments cannot often be observed without major interruptions because of their large, sudden brightness fluctuations. Finally, the rates of the fragments’ relative motions are temporally nonuniform, so that their separation times cannot be ascertained by a linear extrapolation back in time. This approximation invariably leads to a grossly underestimated length of the interval between fragmentation and observation. The solution is likewise made more difficult by the fragmentation hierarchy, in which a fragment of the first generation may become the parent to a fragment of the second generation, etc.

With a high degree of confidence required to prove the relationship between an outburst and a fragmentation event, it is necessary to determine both the onset time of outbursts and the separation time of fragments with high accuracy. If there are several outbursts and several fragments, the timeline of their hierarchy determines the degree of accuracy with which the correspondence between two particular events needs to be resolved.

Well determined onset times of outbursts are also critical in the instances of inadequately observed companions, whose separation times cannot be computed with much accuracy. The outbursts’ onset times are then used to investigate the most probable correlations between outbursts and fragmentation events.

2. THE OUTBURSTS

Any sudden, prominent, and unexpected brightening of a comet, caused by an abrupt, short-term injection of massive amounts of material from the comet’s nucleus into its atmosphere, is called an *outburst*. By *sudden* is meant that the duration of its active stage usually does not exceed a fraction of the day or 1–2 days at the most. The term *prominent* conveys that the overall brightness increase during the event is at least a factor of $2-2\frac{1}{2}$ (an amplitude of not less than 0.8–1.0 magnitude). The word *unexpected* implies that the event is not part of known periodic or quasi-periodic variations, such as due to the nucleus’ rotation. Outbursts, especially the smaller ones, are frequent phenomena experienced over centuries by a large number of comets, some of them discovered while in outburst. The propensity to such flare-ups varies from comet to comet and it is not necessarily correlated with heliocentric distance. It is known that

Comet 29P/Schwassmann-Wachmann (Sec. 2.1), which never gets closer to the Sun than 5.4 AU, undergoes major outbursts repeatedly, with an average rate of 7.4 events per year (Trigo-Rodríguez et al. 2008, 2010).

Ordinary outbursts have some common features with the extremely rare *giant (super-massive) explosions* (e.g., Sekanina 2008a), but in other respects the two categories of phenomena differ from each other. Ordinary outbursts originate, on the nucleus, from discrete active centers (or regions) of a limited extent and always represent *local events* on the scale of the nucleus' dimensions, with the total mass of ejecta below — often by orders of magnitude — 10^{13} grams (e.g., Sekanina 2008a). Even though the mass released during an outburst consists of both gas (active component) and dust, there is a wide range of these events in terms of their mix.

2.1. Historical Highlights: Dust Dominated and Gas Dominated Outbursts

While it is not the goal of this paper to examine possible production mechanisms for cometary outbursts, descriptions of several well documented historical examples of prominent explosive events and a reference to some specific investigations of this subject are relevant to the present objectives.

Critical aspects of explosive events in comets are related to the formation of halos in the coma. Reports of these features date back at least to the early 19th century. The first comprehensive report was from Herschel (1847) in reference to the appearance of comet Halley in late January 1836, observed by him from South Africa with his 47-cm f/13 reflector. Herschel wrote that "...the comet now was indeed a most singular and remarkable object, ... a phenomenon, I believe, quite unique in the history of comets. Within the well-defined head ... was seen a vividly luminous nucleus." Herschel's description of what was the first observed case of a giant explosion (Sekanina 2008b) then continued with many additional details. Most importantly he commented on "the extraordinary sharpness of termination" of the halo and was amazed that "the comet was actually increasing in dimensions with such rapidity that it might almost be said to be seen to grow!" After the event the comet long remained anomalously bright, visible with the naked eye for at least two months. Although no spectroscopic observations were made at the time, it is virtually certain that the halo was composed of microscopic dust.

In 1883–1884 comet 12P/Pons-Brooks experienced a number of outbursts. From a wealth of information in the literature, only a few reports are mentioned below. On one of the events, Struve (1884) in Pulkovo remarked that on September 23, 1883, the comet looked like a star without any nebulosity in a telescope finder but as a round, rather sharply bound mass in the 38-cm refractor. On the subsequent nights this halo grew fainter, larger, and more diffuse and elongated. After five days the feature practically disappeared. From the first three, most reliable measurements of the expanding halo's dimensions reported by Struve, the outburst should have nominally begun on September 22.94 UT, some 2 to $2\frac{2}{3}$ hours after the observations by Schiaparelli (1883) and Abetti (1883), who both reported a very inconspicuous nucleus, but about one hour before the comet was observed at Harvard by Chandler (1883), who was "astonished to

find exactly in [the comet's] place a bright, clearly defined star ... without sensible trace of nebulosity ... that even an experienced observer would easily have failed to distinguish ... from ... stars". Similarly, at about the same time Pickering et al. (1900) commented: "Comet resembles a star. There has been a great change since yesterday." The next night Chandler already saw the nucleus "spread out into a confused, bright disc with ill defined edges." The spectrum taken by Pickering et al. on September 26 showed primarily the molecular bands, with only a faint trace of continuum. The event apparently waned fairly rapidly.

Another major outburst of comet 12P, on January 1, 1884, was witnessed at Potsdam by Vogel (1884) and by Müller (1884a, 1884b). Vogel noticed a dramatic change in the appearance of the comet in a span of two hours, during which a prominent, uniformly luminous, round disk several arcseconds in diameter was formed. Its spectrum was a pure continuum. The dimensions of the disk grew by $4''.1$ in 33 minutes, from which the onset time on January 1.78 UT can be calculated with an estimated uncertainty of not more than a fraction of an hour. This time was only about 1 hour before Vogel's second observation. The disk disappeared on the following days and the continuous spectrum was then restricted only to a tiny nucleus.

Müller's report is of great value, because the outburst occurred literally before his eyes. On January 1.77 UT he noticed that at the location of the diffuse nucleus seen about 90 minutes earlier was now "an almost perfectly point-like star ... at first sight so striking ... [as if] a bright star was about to be occulted by the comet." Müller's magnitude determination of the stellar nucleus with the use of a Zöllner photometer indicated that it still grew in brightness, reaching a fairly flat maximum around January 1.805 UT, then fading gradually. The overall evolution was so rapid that by January 1.90 UT the feature already became distinctly less sharp.

The next extraordinary events were two episodes of a giant explosion experienced by comet 17P/Holmes in 1892–1893. The comet was actually discovered in the course of the first episode, some 45–65 hours after it had begun (as extrapolated from the rate of subsequent expansion; Sekanina 2008a). The spectroscopic observations made soon after the discovery consistently showed the continuous spectrum to dominate, with only a faint band sometimes reported mainly on the outside of the bright disk or halo (Campbell 1893, Kammermann 1893, Vogel 1893). The halo continued to expand to gigantic dimensions, exceeding the Sun's diameter about three weeks after the event's onset. In small instruments the comet's brightness was subsiding at a fairly slow rate, when the beginning of a new explosion was detected by Palisa (1893) some 10 weeks after the first one. He reported (at an estimated 13–23 hours after the onset of the explosion) that the comet looked like "a yellow star, which was surrounded by an envelope $20''$ in diameter." The envelope was a newly formed dust halo. Numerous additional observers provided similar accounts, with their summaries listed elsewhere (e.g., Bobrovnikoff 1943, Sekanina 2008a).

Comet 17P underwent an even more powerful giant explosion in October 2007, when in a matter of about 2 days it brightened by an unprecedented 17 magnitudes (e.g.,

Sekanina 2008a) and was still observed with the naked eye more than $4\frac{1}{2}$ months later! The most conspicuous feature of the post-peak branch of the light curve was a flat plateau, with the total brightness (normalized to 1 AU from the earth) having subsided by only 1 magnitude in the course of 4 months, as measured both by the visual observers (e.g., Sekanina 2008a) and by a red-sensitive CCD detector on the satellite Coriolis (Li et al. 2011). The dust halo was expanding at a rate of 0.5 km/s, losing gradually the symmetry and reaching eventually the dimensions much greater than those of the Sun.

Bobrovnikoff (1932) became interested in the formation of halos in comets after he investigated a number of such expanding features in the head of Halley's comet (Bobrovnikoff 1931). From spectroscopic observations he concluded that they were of gaseous nature. During the 1986 apparition of Halley's comet, Schlosser et al. (1986) imaged the evolution of 15 prominent CN halos (which they called shells) and subsequently Schulz and Schlosser (1990) linked them to CN jets and concluded that they both were made up of CHON particles. Because these features were not associated with a profound brightening of the comet, their nature appears to differ from the halos seen in the early stage of prominent outbursts.

The discovery of Comet 29P/Schwassmann-Wachmann in 1927 provided comet astronomers with an object of unceasing propensity to outbursts, which has ever since been subject for studying these phenomena. The data from the first 10–25 years of observation were summarized by Richter (1941, 1954), who also compared the events in this comet with those in other comets, including 12P/Pons-Brooks and 17P/Holmes (Richter 1949). He concluded that the outbursts of different comets have some common features and presented a timeline of an outburst, which can essentially be summarized into six points:

(1) Before the outburst, the comet generally displays a diffuse coma that sometimes is condensed toward the center and every now and then exhibits a faint stellar nucleus. The spectrum consists of molecular bands.

(2) Within a time interval possibly as short as several minutes or as long as an hour, the comet's appearance is being fundamentally transformed. A brilliant star (a preferable term would be a point-like object — *author*), which triggers a brightening by up to 8 magnitudes, appears in the center. Its spectrum is continuous. The former coma remains partially preserved during the outburst; it may in part be outshined by the star, in part fade away.

(3) Shortly after the outburst, often only several hours later, the stellar nucleus begins to grow steadily into a planet-like disk.

(4) In the course of the next days the disk continues to grow. The comet's total brightness, which during this process has leveled off or still risen, begins now to subside.

(5) After a few more days the comet regains its pre-outburst appearance and so does its spectrum.

(6) The duration of these physical changes differs from case to case. Even though the course of events is the same, the scale of each outburst entails a different time interval.

One may not agree with every detail of this description by Richter (1949), but overall it does appear to recount the individual stages of evolution of outbursts rather credibly.

In the same paper Richter also addressed the issue of expansion velocity, finding values mostly on the order of hundreds of meters per second, and he discussed a few possible production mechanisms.

In the decades since Richter's papers were written, countless numbers of additional outbursts of comet 29P have been observed and studied. An excellent example is Beyer's (1962) account of a prominent outburst in October 1959. The dust halo was observed to expand for more than 30 days at a projected rate of 0.19 km/s, its maximum measurable dimensions reaching almost those of the Sun. The brightening, whose initial rate was extremely steep, terminated about 4 days later, when the comet reached an apparent visual magnitude 10.7. Beyer's results show that during the subsequent 30–40 days the light curve displayed a flat plateau, with the brightness remaining essentially constant, dropping by only 1 magnitude as late as 50–60 days after reaching the peak. It is obvious that this light curve is somewhat reminiscent of that of the giant explosions, except that the flat plateau did not extend for quite as long. Even so, ejected dust with a long residence time in the coma appears to dominate the outbursts of comet 29P, unlike those of 12P.

The light curves of 29P/Schwassmann-Wachmann's outbursts published by Trigo-Rodríguez et al. (2008, 2010) differ from that by Beyer (1962). While the steep brightness jump at the outbursts' onset is as striking as in Beyer's light curve, the peak appears much sharper, with the brightness beginning to drop significantly only days afterwards. This effect is apparently due to the use by Trigo-Rodríguez et al. of a small, 10'' aperture, with which they sample only a fraction of the coma to a distance, on the average, of some 40,000 km from the nucleus. Thus, Beyer's light curve is representative of the comet's total brightness, Trigo-Rodríguez et al.'s light curves illustrate brightness variations merely in the coma region nearer the nucleus. It follows that with an adopted velocity of ~ 0.2 km/s for the coma expansion rate, the aperture covers only dust emissions less than about 50 or 60 hours old. By modeling a major outburst of 29P in February 1981, Sekanina (1990, 1993) established from the feature's morphology that its duration was about 0.7 the rotation period, or 3.5 days with Whipple's (1980) rotation period of 4.97 days. Comparing the time scale of this outburst's evolution with its morphology constraint, the rotation period could hardly exceed, or be much shorter than, 5–6 days. However, most values suggested in the literature are in fact longer (Jewitt 1990, Stansberry et al. 2004, Trigo-Rodríguez et al. 2010); on the other hand, Meech et al. (1993) found a very rapid and complex rotation.

During the past decades, major outbursts have also been observed in a large number of other comets, only a few of them being mentioned below. Comet 41P/Tuttle-Giacobini-Kresák underwent two enormous outbursts, both with an amplitude of ~ 9 magnitudes, 41 days apart during its 1973 apparition (Kresák 1974). Spectroscopic data showed that the second outburst was dominated by molecular emissions (C_2 , C_3 , CN, CH), with only a weak to medium-strength continuum present (Swings

and Vreux 1973). However, from the similarities in the coma morphology, duration (3 and 2 days, respectively; Kresák 1974), light curve (the rate of brightness subsidence only moderately gentler than the rate of rise), and other attributes, it is likely that both outbursts were gas dominated, resembling those of comet 12P. The domination by gas in the second outburst is also consistent with the absence of any major increase in the brightness at close proximity of the nucleus and any sharply-bounded halo around the time of the maximum total brightness; with the shrinking of the bright coma from 110,000 km to 16,000 km in diameter between 2 and 3 days after the onset of the second outburst; and with the detection of a *diffuse* nuclear condensation 3400 km in diameter at the first of the two times (Kresák 1974). Comet 41P also experienced a rarely mentioned postperihelion outburst during its 1995 return (Green 1995) and three preperihelion outbursts within a span of about three weeks during its 2000/2001 apparition (e.g., Sekanina 2008a).

Another previously faint periodic comet, 73P/Schwassmann-Wachmann, entered its explosive era shortly before perihelion of its 1995 return, when it underwent a 5-magnitude outburst, first detected — on account of the comet’s proximity to the Sun in the sky — with a radiotelescope (Crovissier et al. 1996). While no spectrum in the visible light is available, it appears that no observable halo was formed during the outburst, which accompanied a multiple fragmentation of the parent nucleus (Sekanina 2005). The comet’s nuclear companions from 1995 continued to fragment during the fabulously favorable apparition of 2006 and probably also during the intervening return of 2000/2001, when the comet was observed less extensively.

The complex correlation between nuclear fragmentation and outbursts was exemplified by comet C/2001 A2 (LINEAR). The parent nucleus — also called component B — split, step by step, to generate six companions, A and C–G, and underwent four outbursts, I–IV (Sekanina et al. 2002, Jehin et al. 2002). Outburst I coincided with the birth of companion A, outburst II with companion C, and outburst III with companions D, E, and F. Outburst IV was not observed to correlate with any nuclear fragment, while the birth of fragment G was not accompanied by any outburst. According to Sekanina et al. (2002), a fragmentation event is or is not accompanied by an observable outburst, depending on whether or not a significant fraction of the fragment’s mass disintegrates into dust upon separation; and an outburst with no observed fragmentation event is the outcome of the fragment’s complete (or near-complete) disintegration. These scenarios need to be kept in mind in the following investigation of comet 168P.

From the wealth of information on exploding comets, it is concluded that an outburst as such has no diagnostic significance for predicting the future evolution of the object. After undergoing an outburst, many comets do not change their behavior at all. For others, an outburst triggers an extended period of enhanced activity, whereas for the unfortunate few it portends their imminent cataclysmic demise. Such terminal flare-ups were exhibited, for example, by comets C/1999 S4 (LINEAR) and C/1996 Q1 (Tabur) shortly before their disintegration, but the sequence of events observed in comet 168P is inconsistent with a “doomsday” scenario.

The above examples of explosive phenomena in comets amply demonstrate that observationally *each* such event begins exactly the same way, with the appearance in the middle of the coma of a bright *starlike object*, whose first sighting coincides with the onset of a *precipitous rise* in the brightness of the central coma. This stellar feature is an initial stage of an expanding halo (or disk) of material, whose surface brightness gradually decreases until its eventual disappearance, while its integrated brightness may for a while continue to increase with time, depending on the amount of released material, on the relative contributions from gas and dust, on the size-distribution of dust particles, and on the post-outburst physical conditions in the active region from which the outburst originated. When the outburst is dominated by gas, the rate at which the brightness generally subsides is determined primarily by the photodissociation lifetime of the observed molecules (such as C₂, CN, etc., in the visible light), which does not exceed a day or two near 1 AU from the Sun. However, these photodissociation products, contributing substantially to the brightness of the outer coma, do not have any effect on the region of nuclear condensation, where ejected dust appears to prevail even in the gas dominated outbursts. Because of smaller amounts of dust involved, the post-peak comet brightness in these events drops more rapidly with time and the expanding disk disappears soon. By contrast, when the outburst is dominated by dust, the brightness subsides more gradually and the expanding dust halo, while changing its morphology, survives longer.¹ If the outburst triggers an episode of continuing dust emission from the source or nearby areas on the nucleus, the brightness may remain elevated for an extended period of time. Finally, the shape of the light curve also depends on the comet’s position in the orbit (preperihelion vs. postperihelion, heliocentric distance, etc.) and on the diurnal and/or seasonal activity variations at the location of the emission region.

2.2. Outbursts and the Nuclear Magnitudes

The purpose of this paper is to convince the reader that CCD data sets of the nuclear-condensation brightness (not to be confused with the true brightness of the comet’s nucleus), routinely reported in terms of the so-called *nuclear magnitudes* to the IAU Minor Planet Center (MPC) as part of astrometric observations, can serve as the basis to a simple, straightforward technique for efficiently constraining the onset time of outbursts.

Given the poor reputation of *reported nuclear magnitudes*, this statement appears at first sight to be nothing short of heresy. Indeed, in smaller telescopes the nucleus is always hidden in a much brighter condensation that surrounds it, and the observer is in no position to rectify the problem. It gets so bad that, for example, the glossary of the *International Comet Quarterly (ICQ)*,² emphasizes that these magnitudes are “fraught with problems . . . especially because [they] are extremely dependent upon instrumentation . . . and wavelength. Nuclear magnitudes are chiefly used for astrometric purposes, in

¹ The dust halos originating in the giant explosions survive by far the longest.

² Consult the subject items “m₂” and “Magnitude” in the ICQ web site <http://www.icq.eps.harvard.edu/ICQGlossary.html>.

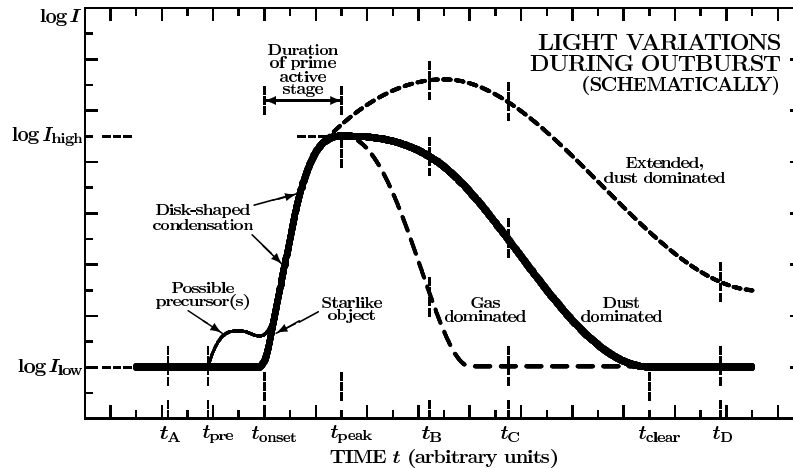


Figure 1. Schematic representation of an outburst. The brightness, I , is plotted on a logarithmic scale against time t . Three categories of events are depicted: a “standard” dust dominated (solid curve), an extended dust dominated (short-dashed curve), and a gas dominated (long-dashed curve). All three events begin at the same onset time, t_{onset} , when the brightness is I_{low} . The precipitous rise in the brightness, which includes the appearance of the starlike object at the location of the nucleus and, later, the appearance of the disk-shaped condensation, is terminated at time t_{peak} , the end of the prime active stage, when I reaches a maximum, I_{high} . The brightness then begins to subside at a slower rate, until it drops to the quiescent level I_{low} at time t_{clear} . By this time, all material ejected during the outburst has left the volume of coma photometrically investigated. For an extended dust dominated outburst, the coma continues to brighten after t_{peak} and its brightness may remain elevated after t_{clear} because of a persisting higher production rate of dust. For the gas dominated outburst, the brightness subsides more rapidly, reaching I_{low} long before t_{clear} . The main outburst may be preceded by a minor precursor (thin curve), which starts at t_{pre} . The symbol I refers normally to the comet’s total brightness, but it could also apply to the brightness I_N of the nuclear condensation. The scenario is the same, but the rate of subsidence would then be generally steeper.

which predictions are made for the brightness of the comet’s nuclear condensation so that astrometrists can gauge how faint the condensation is likely to be and thus how long an exposure is needed to get a good, measurable image . . . [of] the site of the main mass of any comet.”

As also mentioned in the ICQ glossary, the nuclear magnitudes of comets used to be designated as m_2 in the ephemerides of comets, but “in 2003 a subcommittee of IAU Commission 20 . . . decided that the concept of ‘nuclear’ magnitudes should be done away with . . . [and] since then the heading ‘Mag.’ . . . refer[s] to the predicted brightness of comets.” Whereas comet ephemerides no longer provide *predicted* values of nuclear magnitudes, the MPC’s report format for the optical astrometric observations of comets to be submitted for publication in the *Minor Planet Circulars* and the *Minor Planet Electronic Circulars*³ continues to allow one to list the nuclear magnitudes with a flag “N” (as opposed to “T” for the “total” magnitudes) in column 71. A great majority of comet observers has indeed to this day been providing the nuclear magnitudes of comets in this fashion.

The sudden appearance, at the location of the nucleus, of the starlike object signals the beginning of release from the surface of a major plume of material, activated by a surge of erupting gases from the underneath. Measured with a small sampling aperture, the nuclear magnitude is much more sensitive to both the initial starlike stage of the outburst and to the steep brightening of the expanding plume (that is, the halo) than is the comet’s total magnitude. Hence, the same property of the nuclear magnitudes that makes them unattractive for other scientific studies is now deliberately exploited. To my knowledge, this approach has never been employed before. In practice, caution need be exercised in examining

the published information, because the *nuclear magnitude* H_N — the quantity used to characterize the brightness I_N of the nuclear condensation — may, as already pointed out, vary from observer to observer. Two caveats deserve particular attention:

- (1) It is inadmissible to combine sets of nuclear magnitudes H_N , reported by different observers, unless they are *proven* to be compatible by careful analysis; and
- (2) The detection of an outburst can only be regarded as secure, if the timing of its onset is consistently and independently confirmed by all, or at least an overwhelming majority of, the relevant sets of nuclear-magnitude data reported by the observers during the critical period of time.

On the other hand, a great advantage of this approach is the fact that information on the nuclear-condensation brightness is listed by nearly all observers who report their astrometric results. Accordingly, for most comets, including 168P, extensive sets of CCD nuclear magnitudes are available for application of this technique.

2.3. Temporal Photometric Profile of an Outburst

Schematically, the brightness variations during an outburst are expected to follow one (or be a combination) of the light curves in Figure 1. The solid curve is a generic brightness profile for a dust dominated outburst. The event starts at time t_{onset} , when the bright stellar object first appears at the location of the nucleus and the sheer brightness rise begins. The starlike feature is the initial stage of an expanding luminous disk, whose brightness peaks at t_{peak} . The quantity $2.5 \log(I_{\text{high}}/I_{\text{low}})$ is the amplitude of the outburst in magnitudes, whereas the interval $t_{\text{peak}} - t_{\text{onset}}$ is the duration of its prime active stage, assuming that it is shorter than the residence time of dust particles within the measured boundaries of the coma and that the luminous disk is optically thin (as is almost always the case even near the nucleus itself), and

³ See the information web site of the IAU Minor Planet Center <http://www.minorplanetcenter.net/iau/info/OpticalObs.html>.

in the absence of dust fragmentation. At t_{peak} the brightness begins to subside, first very slowly, until it eventually drops to the quiescent level I_{low} at time t_{clear} . By this time, the withdrawal from the volume of the coma of all material ejected during the outburst is completed. With the next event, the whole cycle is repeated.

The brightness of an extended dust dominated outburst continues to rise after t_{peak} because of a persisting higher production rate of dust (or for another reason, such as dust particle fragmentation). For example, the prime event may be followed by secondary outbursts (caused, e.g., by impacts of boulders in ballistic trajectories back on the surface, thus opening new emission centers), which in some cases could lead to more or less permanently elevated activity, continuing to fill the coma with large amounts of new dust.

In the gas dominated outbursts the post-peak brightness subsides more rapidly than in the dust dominated outbursts, reaching I_{low} long before t_{clear} . The halo, containing dust, disappears soon after the outburst's onset.

The prime active stage of any outburst may be preceded by a precursor, a minor flare-up that indicates that the main event is in the making. Since an outburst is essentially the product of succumbing to a stress applied to the surface at a particular location of the nucleus, the precursor could very well be the sign of the nucleus' limited initial resistance to the straining force.

In this subsection, the brightness I — as well as I_{low} and I_{high} — has been understood to refer to the coma, or, more precisely, to the coma within its measured boundaries. Since there are no constraints on the boundaries, I is, generically, the brightness in any volume of the coma centered on the nucleus, and may therefore also indicate I_N [and similarly $(I_N)_{\text{low}}$ and $(I_N)_{\text{high}}$], the brightness of the nuclear condensation, as derived, in terms of the nuclear magnitude H_N , from the measurements of the CCD images through a small sampling aperture.

2.4. Method for Constraining the Onset Time of an Outburst from Sets of Nuclear Magnitudes

I now consider a dust dominated outburst (solid curve in Figure 1) and a set of nuclear-brightness data, $(I_N)_j$ ($j = 1, 2, \dots$), reported by a particular observer. Let the first k observations be made before the outburst's onset, so that at any time t_j ($j = 1, 2, \dots, k$) that satisfies a condition $t_j < t_{\text{onset}}$, such as t_A in Figure 1, the expected nuclear brightness is $(I_N)_j \simeq (I_N)_{\text{low}}$. Let the next $n - k$ observations be made, by the same observer with the identical telescope, after the outburst's onset, but before all dust ejecta evacuate the region of the nuclear condensation whose brightness the observer measures. These times satisfy a condition $t_{\text{onset}} < t_j < t_{\text{clear}}$ ($j = k + 1, k + 2, \dots, n$), such as t_B or t_C in Figure 1, and the brightness is then $(I_N)_{\text{low}} < (I_N)_j \leq (I_N)_{\text{high}}$. Perfunctory inspection of the set of nuclear-brightness data usually suffices to detect the sudden jump in I_N between times t_k and t_{k+1} and to conclude that the outburst began at some point between the two times,

$$t_k < t_{\text{onset}} < t_{k+1}. \quad (1)$$

This result, derived from the particular observer's data, formally provides the expressions for a probable time of the outburst's onset, $\langle t_{\text{onset}} \rangle = \frac{1}{2}(t_k + t_{k+1})$, and its uncertainty, which is equal to $\pm \frac{1}{2}(t_{k+1} - t_k)$. It is noted

that no information on the outburst can be extracted from observations made at times $t_j > t_{\text{clear}}$, that is, at $j > n$, such as at t_D in Figure 1. If no observation has been made between t_k and t_{n+1} , that is, when $n = k$, the observer has missed the outburst.

Next, I consider a total of ν observers that provide information on the comet's nuclear brightness before and during the outburst. Let the brightness data by an i th observer ($i = 1, \dots, \nu$) constrain, in analogy to condition (1), the outburst's onset time to an interval $t_i^- < t_{\text{onset}} < t_i^+$, and let the set of all times between t_i^- and t_i^+ be called \mathbf{A}_i ,

$$\mathbf{A}_i = (t_i^-, t_i^+), \quad (2)$$

where the parentheses mean an open interval, with the boundaries excluded. The resulting constraint, obtained by combining those from the data by all ν observers, is then represented by the intersection \mathbf{A} of the sets \mathbf{A}_i ,

$$\mathbf{A} = \bigcap_{i=1}^{\nu} \mathbf{A}_i = (\max[t_1^-, t_2^-, \dots, t_\nu^-], \min[t_1^+, t_2^+, \dots, t_\nu^+]). \quad (3)$$

Thus, while the brightness data by the individual observers should not be mixed, the temporal constraints derived from them can readily be combined.

Valid constraints can be obtained even from the sets of nuclear-brightness data by the observers who saw the comet only before t_{onset} or only after t_{onset} (but before t_{clear} , of course), once one knows the tentative constraints on the onset time from the data sets by other observers. If all of the brightness data reported by an observer p ($p \leq \nu$) at times close to this range are near his own $(I_N)_{\text{low}}$ value, then his last observation, made at time t_p^- , can be incorporated into condition (3) as a valid constraint. Similarly, if all of the brightness data reported by an observer q ($q \leq \nu$) at times close to this range are much greater than his own $(I_N)_{\text{low}}$ value, then his first observation, made at time t_q^+ , can likewise be incorporated into condition (3) as a valid constraint. On the other hand, the times t_p^+ and t_q^- , referring to these observers' missing brightness constraints at the other end of the time interval, are obviously indeterminate, can be put equal to, e.g., $t_p^+ \rightarrow +\infty$ and $t_q^- \rightarrow -\infty$, and have no effect on the condition (3). The expression for the probable onset time of the outburst and its uncertainty resulting from the applied set of constraints is finally

$$\langle t_{\text{onset}} \rangle = \frac{1}{2} \{ \max[t_1^-, t_2^-, \dots, t_\nu^-] + \min[t_1^+, t_2^+, \dots, t_\nu^+] \} \\ \pm \frac{1}{2} \{ \min[t_1^+, t_2^+, \dots, t_\nu^+] - \max[t_1^-, t_2^-, \dots, t_\nu^-] \}, \quad (4)$$

where $\min[t_1^+, \dots] > \max[t_1^-, \dots]$. This concludes the exercise.

3. COMET 168P/HERGENROTHER IN 2012

Discovered by C. W. Hergenrother in November 1998 on images taken by T. B. Spahr, this short-period comet with a perihelion distance of 1.4 AU remained very faint during its observed returns to perihelion in 1998 and 2005.⁴ In 2012, an extremely favorable return, its apparent magnitude was expected to reach 15 near perihelion, which occurred on October 1.

⁴ See, e.g., <http://cometography.com/pcomets/168p.html>.

Table 1. A list of sources for nuclear magnitudes of comet 168P.

Site code	Observing site ^a	Observer(s) ^b	Instrumentation ^c
160	Osservatorio di Castelmartini, Larciano, Italy	M. Jäger, E. Prosperi <i>et al.</i>	35-cm f/10 T
213	Observatorio Montcabrer, Spain	R. Naves	30-cm f/10 T
215	Volkssternwarte Buchloe, Germany	W. Hasubick	44-cm f/4.6 L
510	Sternwarte der Universität Siegen, Germany	K.-F. Osterhage, H. Bill <i>et al.</i>	43-cm f/6.8 L
585	Kiev Comet Station, Ukraine	A. Baransky, A. Vorontseva	70-cm f/4 L
850	Cordell-Lorenz Observatory, Sewanee, Tennessee, U.S.A.	D. T. Durig, J. R. Adams <i>et al.</i>	30-cm f/2.4 T
945	Observatorio Monte Deva, Gijón, Spain	J. R. Vidal	36-cm f/4.5 T
954	Observatorio del Teide, Tenerife, Canary Islands, Spain	N. E. Pritchett, N. Paul	{ 35-cm f/11 T 50-cm f/6.8 L
958	Observatoire de Dax, France	P. Dupouty, J. B. de Vanssay	{ 20-cm f/3.3 T 30-cm f/6.3 T 43-cm f/3.5 L
A24	New Millennium Observatory, Mozzate, Italy	E. Cozzi	36-cm f/11 T
A71	Stixendorf, Austria	M. Jäger, E. Prosperi <i>et al.</i>	{ 20-cm f/2.8 L 25-cm f/3.8 L 35-cm f/3.1 L 35-cm f/4.1 L
A77	Observatoire Chante-Perdix, Dauban, France	C. Rinner, F. Kugel <i>et al.</i>	{ 8-cm f/7.5 R 40-cm f/3 L
B50	Comer Observatory, Durmersheim, Germany	J. Linder	20-cm f/11.3 T
B53	Casal Lumbroso, Rome, Italy	D. Pivato	19-cm f/4.0 L
B59	Borken, Germany	C. Overhaus	10-cm f/9 R
B70	Sant Celoni, Spain	L. Montoro	20-cm f/4 T
B96	Brixiais Observatory, Kruikeke, Belgium	E. Bryssincks	40-cm f/3.8 A
C10	Maisoncelles, France	J.-F. Soulier	{ 9-cm f/5.3 M 30-cm f/3 L
C23	Olmen, Belgium	A. Diepvens	20-cm f/9 R
C36	Starry Wanderer Observatory, Baran', Belarus	S. Shurpakov	20-cm f/4.0 S
C47	Nonndorf, Austria	G. Dangl	25-cm f/4.8 L
C86	Blanes, Spain	J. Gaitan	25-cm f/6.8 L
C90	Vinyols, Spain	L. Tremosa	20-cm f/5 L
D09	Observatory Grömme, Maasmechelen, Belgium	P. Dekelver	20-cm f/4.5 L
G26	Fushan Observatory, Mt Shaohua, China	W. Pei	20-cm f/4 L
H06	iTelescope Observatory, Mayhill, New Mexico, U.S.A.	M. Suzuki, H. Sato <i>et al.</i>	{ 25-cm f/3.3 L 25-cm f/3.4 A 43-cm f/6.8 A + f/4.5 focal reducer 51-cm f/6.8 A + f/4.5 focal reducer
H45	Petit Jean Mountain South, Arkansas, U.S.A.	P. C. Sherrod	51-cm f/4.3 A
H47	Vicksburg, Mississippi, U.S.A.	C. Bell	30-cm f/10 T + f/4.7 focal reducer
I57	Elche, Spain	J. Lozano	25-cm f/10 T
I72	Observatorio Carpe-Noctem, Madrid, Spain	J. L. Martín	10-cm f/6.0 R
I79	AstroCamp, Nerpio, Spain	T. Lopez	20-cm f/5.2 L
I81	Tarbatness Observatory, Portmahomack, Scotland, U.K.	D. Buczynski	35-cm T + f/6 focal reducer
I88	Fuensanta de Martos, Spain	J. Carrillo	36-cm f/5 L
I99	Observatorio Blanquita, Vaciamadrid, Spain	F. Limon	20-cm f/3.3 T
J01	Observatorio Cielo Profundo, Oviedo, Spain	J. Gonzalez	23-cm f/5 T
J08	Observatorio Zonalunar, Puzol, Spain	A. Carreño	20-cm f/5 L
J24	Observatorio Altamira, Tenerife. Canary Islands, Spain	J. F. Hernandez	40-cm f/10 T
J36	Observatorio DiezALaOnce, Illana, Spain	F. G. Pinilla	25-cm f/4 T
J38	Observatorio La Vara, Valdés, Spain	F. García	25-cm f/8.1 Y
J47	Observatorio Nazaret, Lanzarote, Canary Islands, Spain	G. Muler	30-cm f/10 T

^a Taken from <http://www.minorplanetcenter.net/iau/lists/ObsCodesF.html>.

^b First two observers, as listed with the chronologically summarized observations in the *Minor Planet Circulars; et al.* marks additional observers.

^c Abbreviations for the telescope type, as used in the ICQ and defined in Green (1997). Specifically: A = astrograph, L = Newtonian reflector, M = Maksutov-Cassegrain, R = refractor, S = Schmidt-Newtonian, T = Schmidt-Cassegrain, and Y = Ritchey-Chrétien.

The first published indication of a major deviation from the expected evolution was a visual observation by Gonzalez (2012), who reported the comet to be of magnitude 11.2 in his 20-cm reflector on September 6.90 UT. The comet then continued to brighten, reaching a total magnitude of at least 9 during October (e.g., Green 2012). The comet was more than 4 magnitudes brighter than expected in early September and at least 6 magnitudes brighter than expected during October.⁵

⁵ The predicted magnitudes are at the *Cometary Science Laboratory's* site: <http://www.csc.eps.harvard.edu/168P/index.html>.

3.1. The Outbursts of Comet 168P

Applying the described method, I was able to detect not one, but three consecutive outbursts of this comet in a time span of one month. The search began by collecting the sets of nuclear magnitudes reported to the MPC by the astrometric observers from 40 locations (Spahr et al. 2012). Information on these observing sites is summarized in Table 1, the individual columns listing successively: the IAU site code (as assigned by the MPC), the observatory's name and/or location, the name(s) of the observer(s), and the instrumentation used.

The sets of input data for the outburst search are presented in Tables 2–5. Tables 2–4 have identical format and list the data sets relevant to, respectively, outbursts I, II, and III. In each of these tables the data are arranged by the observatory in column 1, with the dates of observation, t_{obs} , following in column 2 chronologically. More specifically, because it is customary to take several images during each night, it is the interval from the mid-exposure time of the first image to the mid-exposure time of the last image that is listed to 0.001 of a day. This interval usually amounts to a fraction of one hour, but there are exceptions, with a longer span sometimes covered. Occasionally, long sequences of images were taken, in which case more data sets are tabulated for the same date. Each interval is then converted to a range of times reckoned from the comet’s perihelion time, t_{π} , in column 3. Columns 4, 5, and 6 show, respectively, the nuclear magnitude $\langle H_N \rangle$, calculated as an average of the magnitudes from the individual images provided by the observer(s), its root-mean-square error, and the number of images reported. The same nuclear magnitude from all images is marked by a dash in column 5. The final column, one line per observing site, provides the constraint, in terms of a range of allowed onset times, resulting from the sets of images taken at the given observing site and reckoned again from the perihelion time. The relationship of these constraints to the terms used in the method from Sec. 2.4 is discussed in the next paragraph. In addition, each outburst is described by an *average magnitude jump*, calculated from the tabulated differences in $\langle H_N \rangle$ that bracket the derived onset time. This quantity is a crude measure, on the magnitude scale, of the outburst’s perceptibility. It is useful for assessing a level of one’s confidence that the outburst occurred (the greater the jump, the more confident one feels), but does not characterize its strength and has no direct relationship to the amount or mass of the material ejected in the event.

If the entry in column 7 consists of two numbers, they indicate, respectively, times $t_i^- - t_{\pi}$ and $t_i^+ - t_{\pi}$, where t_i^- and t_i^+ are the boundaries of the set \mathbf{A}_i in equation (2) and t_{π} is the comet’s perihelion time. For example, in the data set from observing site A71 for outburst I in Table 2, the images from the first three dates — on August 15, August 28, and September 9 — give the average nuclear magnitudes of 16.9, 17.5, and 15.5, each with an uncertainty of ± 0.1 magnitude. According to the observers at this site, the nuclear condensation apparently faded a little between the first two dates, with no evidence of an outburst prior to, and including, August 28.039 UT. However, the brightness jumped up by fully 2 magnitudes between that time and September 9.865 UT, the time of the first image on the 9th, so the outburst must have occurred in the intervening period of time. This is consistent with Gonzalez’s (2012) observation mentioned above. When reckoned from the perihelion time, August 28.039 UT is equivalent to -34.933 days, while September 9.865 UT becomes -22.107 days, which are indeed the two entries listed as the boundary constraints for the onset of outburst I in the last column of Table 2 from the nuclear magnitudes provided by site A71. To call the reader’s attention to the magnitude jump, the entries in column 7 are positioned between the rows of the two boundary dates and, in addition, a wedge separates these two rows in the nuclear-magnitude column.

If the data reported in Table 2 by observing site A71 were the only constraint available, the probable onset time of outburst I, would have been, following (4) and after rounding off, $\langle t_{\text{onset}} \rangle = \text{September } 3.5 \pm 6.4 \text{ UT}$, or $\langle t_{\text{onset}} \rangle - t_{\pi} = -28.5 \pm 6.4$ days. Table 2 shows, however, that there is a total of 12 constraints, which narrow down the uncertainty considerably and offer for the onset time the tightest limits, which are shown by the entries in the slanted type style in column 7: the maximum value of t_i^- comes from observing site 958, the minimum value of t_i^+ from site C86. The result, in Table 6, shows that the outburst began most probably on September 1, two days earlier than indicated above by the constraints from site A71, and that the uncertainty is more than 4 times smaller. The average magnitude jump from the 9 two-sided constraints is 1.7 ± 0.6 magnitudes, and the first detection of the outburst by Gonzalez (2012) apparently occurred between about 4 to 7 days after it had begun.

The results reported by observing sites C86, D09, and J01 are examples of the post-outburst observations that could be incorporated into Table 2 as further constraints on outburst I, because in each case the nuclear condensation was fading within enough time (5–12 days) after the event. Of these, C86 was in fact instrumental in reducing the error of the result, because no other observations were made on September 3 and the comet was not observed at all on September 1, 2, and 4.⁶

Outburst II, for which the input data are summarized in Table 3, differed from outburst I in that it clearly had a precursor. The total number of constraints on the timing of the main event equals 14, described again in column 7. The maximum value of t_i^- comes from site H47 and the minimum value of t_i^+ from site C47. For each of the 14 sites, a large wedge marks the outburst in the column for the nuclear magnitudes. From sites H47 and I81 the comet was observed only before the outburst’s onset, from site I57 only after it. From the 11 two-sided constraints the average magnitude jump equals 2.4 ± 0.6 magnitudes; the resulting onset time is in Table 6.

The precursor to outburst II appears in six of the 14 data sets in Table 3, from sites 958, C36, C47, I72, I81, and J24. The precursor’s constraints, not listed in Table 6, are marked by the small wedges in column 4 of Table 3. It appears that the precursor began most probably just before September 20.0 UT, more than 2 days before did the main event. The precursor does not show up distinctly in the nuclear magnitudes from C23 and it is not detected in the magnitudes from the other sites, in part because of their unfavorable timelines. The data from sites H47 and J24 suggest that elevated activity culminating in outburst II may have begun even before September 19 (small wedges with a question mark), but this is not supported by the other tabulated data. In any case, there is no doubt that the dust emission rate during much of September was increasing first gradually, before eventually erupting in outburst II. From the six detections of the precursor, its resulting magnitude jump is found to be, on the average, 0.7 ± 0.2 magnitude.

Outburst III is the most difficult test of the proposed technique for detecting the timing of these events, because it has by far the smallest amplitude of the three.

⁶ See the list of astrometric observations of 168P in the MPC database on http://www.minorplanetcenter.net/db_search.

Table 2. Constraints on the onset time for outburst I of comet 168P from nuclear magnitudes.

Site code	Observation times t_{obs} (2012 UT)	Range of times $t_{\text{obs}} - t_{\pi}$ (days)	$\langle H_N \rangle$ (mag)	RMS (mag)	No. obs.	Range of onset times $t_{\text{onset}} - t_{\pi}$ (days)
160	Aug. 29.134–29.139	−33.838 ⇔ −33.833	16.4	±0.1	3	−33.833 ⇔ −22.956
	Sept. 9.016–9.021	−22.956 ⇔ −22.951	15.4	0.1	3	
	16.949–16.953	−15.023 ⇔ −15.019	15.1	0.1	3	
585	Aug. 23.012–23.018	−39.960 ⇔ −39.954	17.0	±0.1	7	−39.954 ⇔ −19.050
	Sept. 12.922–12.930	−19.050 ⇔ −19.042	14.2	0.0 ₄	6	
	12.932–12.935	−19.040 ⇔ −19.037	14.4	0.0 ₄	5	
958	Aug. 30.964–31.084	−32.008 ⇔ −31.888	15.7	—	4	−31.888 ⇔ −26.020
	Sept. 5.952–5.978	−26.020 ⇔ −25.994	14.0	±0.1	3	
	6.978–7.004	−24.994 ⇔ −24.968	13.9	0.2	3	
	7.979–8.006	−23.993 ⇔ −23.966	14.2	0.1	3	
	10.058–10.083	−21.914 ⇔ −27.889	14.6	0.1	3	
A71	Aug. 15.044–15.064	−47.928 ⇔ −47.908	16.9	±0.1	4	−34.933 ⇔ −22.107
	28.014–28.039	−34.958 ⇔ −34.933	17.5	0.1	6	
	Sept. 9.865–9.885	−22.107 ⇔ −22.087	15.5	0.1	6	
	10.978–10.989	−20.994 ⇔ −20.983	15.3	—	7	
	15.002–15.004	−16.970 ⇔ −16.968	15.0	0.1	6	
C23	Aug. 18.106–18.117	−44.866 ⇔ −44.855	16.0	±0.3	3	−35.866 ⇔ −26.021
	23.055–23.066	−39.917 ⇔ −39.906	15.5	0.6	3	
	27.091–27.106	−35.881 ⇔ −35.866	15.8	0.1	3	
	Sept. 5.951–5.971	−26.021 ⇔ −26.001	13.9	0.2	3	
	13.987–14.001	−17.985 ⇔ −17.971	14.1	0.2	3	
C47	Aug. 20.027–20.046	−42.945 ⇔ −11.926	17.3	±0.3	5	−34.946 ⇔ −21.983
	28.011–28.026	−34.961 ⇔ −34.946	17.1	0.2	6	
	Sept. 9.989–10.004	−21.983 ⇔ −21.968	16.1	0.1	6	
	10.963–10.983	−21.009 ⇔ −20.989	15.7	0.3	6	
C86	Sept. 3.094–3.100	−28.878 ⇔ −28.872	13.6	±0.1	3	< −28.878
	7.129–7.132	−24.843 ⇔ −24.840	14.1	—	3	
	D09	Sept. 5.968–5.986	−26.004 ⇔ −25.986	14.4	±0.1	3
D09	7.031–7.050	−24.941 ⇔ −24.922	14.7	0.1	3	
	8.973–8.985	−22.999 ⇔ −22.987	14.9	—	3	
	9.933–9.943	−22.039 ⇔ −22.029	15.2	0.2	3	
	H47	Aug. 22.377–22.393	−40.595 ⇔ −40.579	16.3	±0.1	3
23.370–23.384		−39.602 ⇔ −39.588	16.3	0.2	4	
Sept. 9.294–9.304		−22.678 ⇔ −22.668	15.1	0.1	3	
10.370–10.382		−21.602 ⇔ −21.590	14.5	0.1	4	
11.372–11.390		−20.600 ⇔ −20.582	14.5	0.3	3	
J01	Sept. 6.027–6.081	−25.945 ⇔ −25.891	14.5	±0.1	3	< −25.945
	12.928–12.957	−19.044 ⇔ −19.015	14.8	—	3	
	15.062–15.092	−16.910 ⇔ −16.880	14.5	—	3	
J36	Aug. 25.025–25.030	−37.947 ⇔ −37.942	15.7	±0.1	3	−34.944 ⇔ −23.932
	28.026–28.028	−34.946 ⇔ −34.944	15.7	0.1	3	
	Sept. 8.040–8.043	−23.932 ⇔ −23.929	14.1	—	3	
	8.985–8.990	−22.987 ⇔ −22.982	14.3	0.1	3	
J38	15.047–15.049	−16.925 ⇔ −16.923	14.0	—	3	
	Aug. 11.087–11.089	−51.885 ⇔ −20.883	16.4	—	3	
	12.036–12.042	−50.936 ⇔ −50.930	16.4	±0.1	3	
	17.037–17.040	−45.935 ⇔ −45.932	16.3	—	3	
	18.032–18.037	−44.940 ⇔ −44.935	16.4	—	3	
	27.005–27.010	−35.967 ⇔ −35.962	15.8	0.1	3	
	Sept. 13.983–13.984	−17.989 ⇔ −17.988	14.0	0.1	3	−35.962 ⇔ −17.989
15.954–15.956	−16.018 ⇔ −16.016	14.3	—	3		

The relevant data set is in Table 4, which presents the nuclear magnitudes from 13 observing sites. The comet was observed only before the event from site C23 and only after the event from sites 213 and I99. The data from the remaining 10 sites bracket the onset time of the outburst, but two of these sites failed to register it, as discussed later in this paragraph. From the eight remaining constraints, the maximum value of t_i^- amounts to October 1.80 (site A77) and the minimum value of t_i^+ , October 1.78 (site I57). This result is in conflict, albeit marginal, with the condition $\max[t_i^-, \dots] < \min[t_i^+, \dots]$

mentioned below expression (4). Table 4 shows that the observing session at site A77 completely overlapped the shorter session at site I57, and in both cases the reported magnitude jump was only 0.4 magnitude. Most importantly, the magnitudes reported from I57 are fainter than those from A77, so that the sampling aperture used at I57 was probably smaller and the reported nuclear magnitudes are more diagnostic of the innermost-coma region and of the plume of material leaving the surface of the nucleus. Therefore, as listed in Table 6, outburst III must have begun during, or just moments before, the

Table 3. Constraints on the onset time for outburst II of comet 168P from nuclear magnitudes.

Site code	Observation times t_{obs} (2012 UT)	Range of times $t_{\text{obs}} - t_{\pi}$ (days)	$\langle H_N \rangle$ (mag)	RMS (mag)	No. obs.	Range of onset times $t_{\text{onset}} - t_{\pi}$ (days)
585	Sept. 12.922–12.930	−19.050 ⇔ −19.042	14.2	±0.0 ₄	6	−19.037 ⇔ −3.918
	12.932–12.935	−19.040 ⇔ −19.037	14.4 _Δ	0.0 ₄	5	
	28.054–28.058	−3.918 ⇔ −3.914	11.1 _Δ	0.0 ₄	6	
958	Sept. 14.973–15.002	−16.999 ⇔ −16.970	14.1	±0.1	4	−9.955 ⇔ −9.014
	15.965–15.995	−16.007 ⇔ −15.977	14.4	0.2	4	
	16.985–17.015	−14.987 ⇔ −14.957	14.0	0.1	4	
	19.966–19.993	−12.039 ⇔ −11.979	14.0	0.1	4	
	20.984–21.025	−10.988 ⇔ −10.947	13.6 _Δ	—	6	
	21.986–22.017	−9.986 ⇔ −9.955	13.8 _Δ	0.1	6	
	22.958–22.995	−9.014 ⇔ −8.977	12.1	0.2	15	
	23.031–23.056	−8.941 ⇔ −8.916	12.1	0.2	4	
	23.872–23.927	−8.100 ⇔ −8.045	11.7	0.1	12	
C10	Sept. 15.970–16.000	−16.002 ⇔ −15.972	14.0	±0.2	8	−13.937 ⇔ −2.056
	18.014–18.035	−13.958 ⇔ −13.937	14.2	—	3	
	29.916–29.940	−2.056 ⇔ −2.032	11.4 _Δ	0.1	4	
C23	Sept. 13.987–14.001	−17.985 ⇔ −17.971	14.1	±0.2	3	−10.015 ⇔ −3.052
	21.947–21.957	−10.025 ⇔ −10.015	13.7 _Δ	0.1	3	
	28.908–28.920	−3.064 ⇔ −3.052	11.5	—	3	
	29.874–29.881	−2.098 ⇔ −2.091	11.8	0.1	3	
C36	Sept. 12.960–12.968	−19.012 ⇔ −19.004	14.0	±0.4	11	−11.991 ⇔ −3.115
	14.000–14.004	−17.972 ⇔ −17.968	14.2	0.1	8	
	17.013–17.017	−14.959 ⇔ −14.955	14.1	0.1	5	
	19.973–19.981	−11.999 ⇔ −11.991	13.5 _Δ	0.2	10	
	28.857–28.867	−3.115 ⇔ −3.105	10.8 _Δ	0.0 ₃	14	
	30.911–30.915	−1.061 ⇔ −1.057	11.1	0.1	10	
C47	Sept. 16.874–16.884	−15.098 ⇔ −15.088	15.9	±0.1	6	−11.078 ⇔ −9.048
	20.868–20.894	−11.104 ⇔ −11.078	15.2 _Δ	0.2	5	
	22.924–22.938	−9.048 ⇔ −9.034	13.0 _Δ	0.1	7	
C86	Sept. 3.094–3.100	−28.878 ⇔ −28.872	13.6	±0.1	3	−24.840 ⇔ −5.110
	7.129–7.132	−24.843 ⇔ −24.840	14.1 _Δ	—	3	
	26.862–26.866	−5.110 ⇔ −5.106	11.5	—	3	
H47	Sept. 9.294–9.304	−22.678 ⇔ −22.668	15.1 _Δ	±0.1	3	> −9.616
	10.370–10.382	−21.602 ⇔ −21.590	14.5	0.1	4	
	11.372–11.390	−20.600 ⇔ −21.582	14.5	0.3	3	
	22.350–22.356	−9.622 ⇔ −9.616	14.2 _Δ	0.1	4	
I57	Sept. 24.961–24.985	−7.011 ⇔ −6.987	11.4	—	3	< −7.011
	26.027–26.045	−5.945 ⇔ −5.927	11.5	±0.1	3	
I72	Sept. 14.956–14.962	−17.016 ⇔ −17.010	14.0	—	3	−9.913 ⇔ −5.080
	15.996–16.002	−15.976 ⇔ −15.970	14.3	—	5	
	22.054–22.059	−9.918 ⇔ −9.913	13.7 _Δ	±0.1	3	
	26.892–26.898	−5.080 ⇔ −5.074	11.5 _Δ	0.1	3	
I81	Sept. 16.057–16.068	−15.915 ⇔ −15.904	14.5	±0.3	3	> −11.031
	16.991–17.005	−14.981 ⇔ −14.967	14.8	—	2	
	20.934–20.941	−11.038 ⇔ −11.031	13.7 _Δ	0.1	2	
J01	Sept. 15.062–15.092	−16.910 ⇔ −16.880	14.5	—	3	−16.880 ⇔ −5.106
	26.866–26.904	−5.106 ⇔ −5.068	11.7	±0.1	3	
	29.957–29.979	−2.015 ⇔ −1.993	12.1	0.1	3	
	30.909–30.949	−1.063 ⇔ −1.023	11.9	0.2	3	
J24	Sept. 13.194–13.208	−18.778 ⇔ −18.764	14.6	±0.1	3	−9.849 ⇔ −8.987
	19.172–19.186	−12.800 ⇔ −12.786	14.1 _Δ	0.1	3	
	22.114–22.123	−9.858 ⇔ −9.849	13.5 _Δ	—	3	
	22.985–23.016	−8.987 ⇔ −8.956	12.1	0.1	3	
	25.922–25.929	−6.050 ⇔ −6.043	11.4	0.1	3	
	27.121–27.125	−4.851 ⇔ −4.847	11.4	0.1	3	
J38	Sept. 13.983–13.984	−17.989 ⇔ −17.988	14.0	±0.1	3	−16.016 ⇔ −1.097
	15.954–15.956	−16.018 ⇔ −16.016	14.3	—	3	
	30.875–30.879	−1.097 ⇔ −1.093	11.4 _Δ	—	3	

observing session at site I57, and the onset time is determined with accuracy better than ± 0.1 day. The minor discrepancy between the constraints from sites I57 and A77 illustrates that the recognition of an outburst's onset depends, to a degree, on the details of imaging observations (Sec. 3.2). As already mentioned, outburst III was not detected at two of the 13 sites, J08 and J24, even though in both cases the observations do bracket the onset time established by the data from the other

sites (Table 4). Closer inspection shows a 7-day gap between the two J08 entries that bracket outburst III, the first having been made during, or shortly after, outburst II. Similarly, the second of the two J24 observations that bracket outburst III was made on October 6, more than 4 days after the event's onset. These cases illustrate the advantage of having a dense timeline. Indeed, every site that provided consistent constraints featured at least one observation from the time span of October 1–4.

Table 4. Constraints on the onset time for outburst III of comet 168P from nuclear magnitudes.

Site code	Observation times t_{obs} (2012 UT)	Range of times $t_{\text{obs}} - t_{\pi}$ (days)	$\langle H_N \rangle$ (mag)	RMS (mag)	No. obs.	Range of onset times $t_{\text{onset}} - t_{\pi}$ (days)
213	Oct. 2.848–2.857	+0.876 \Leftrightarrow +0.885	11.0 ∇	—	3	<+0.976
	5.855–5.861	+3.883 \Leftrightarrow +3.889	11.3	—	3	
	7.909–7.910	+5.937 \Leftrightarrow +5.938	11.4	—	2	
	8.916–8.926	+6.944 \Leftrightarrow +6.954	11.5	± 0.1	3	
958	Sept. 23.872–23.927	–8.100 \Leftrightarrow –8.045	11.7	± 0.1	12	–0.997 \Leftrightarrow –0.073
	24.846–25.010	–7.126 \Leftrightarrow –6.962	11.6	0.1	10	
	28.129–28.160	–3.843 \Leftrightarrow –3.812	11.4	0.1	9	
	30.897–30.975	–1.075 \Leftrightarrow –0.997	11.4 ∇	0.1	15	
	Oct. 1.899–1.948	–0.073 \Leftrightarrow –0.024	11.0 ∇	0.1	6	
	2.936–2.980	+0.964 \Leftrightarrow +1.008	10.9	0.1	6	
	3.875–3.906	+1.903 \Leftrightarrow +1.934	11.0	0.1	3	
	4.927–4.959	+2.955 \Leftrightarrow +2.987	11.3	0.0 ₄	5	
	5.933–5.962	+3.961 \Leftrightarrow +3.990	11.3	0.1	4	
	7.059–7.080	+5.087 \Leftrightarrow +5.108	11.2	0.1	3	
7.909–7.939	+5.937 \Leftrightarrow +5.967	11.0	0.1	4		
A77	Sept. 26.969–26.996	–5.003 \Leftrightarrow –4.976	10.8	± 0.1	3	–0.172 \Leftrightarrow +5.761
	Oct. 1.778–1.800	–0.194 \Leftrightarrow –0.172	10.7 ∇	—	3	
	5.761–5.777	–3.789 \Leftrightarrow –3.805	10.3 ∇	—	3	
C23	Sept. 28.908–28.920	–3.064 \Leftrightarrow –3.052	11.5	—	3	> –1.005
	29.874–29.881	–2.098 \Leftrightarrow –2.091	11.8	± 0.1	3	
	30.958–30.958	–1.014 \Leftrightarrow –1.005	11.7 ∇	0.1	3	
C36	Sept. 28.857–28.867	–3.115 \Leftrightarrow –3.105	10.8	$\pm 0.0_3$	14	–1.057 \Leftrightarrow +2.840
	30.911–30.915	–1.061 \Leftrightarrow –1.057	11.1 ∇	0.1	10	
	Oct. 4.812–4.820	+2.840 \Leftrightarrow +2.848	10.3 ∇	0.1	14	
	5.817–5.833	+3.845 \Leftrightarrow +3.861	10.3	0.2	11	
C47	Sept. 22.924–22.938	–9.048 \Leftrightarrow –9.034	13.0	± 0.1	7	–9.034 \Leftrightarrow +0.861
	Oct. 2.833–2.846	+0.861 \Leftrightarrow +0.874	12.5 ∇	0.2	6	
	11.942–11.948	+9.970 \Leftrightarrow +9.976	13.1	0.4	5	
	13.972–13.986	+12.000 \Leftrightarrow +12.014	13.3	0.2	7	
I57	Sept. 24.961–24.985	–7.011 \Leftrightarrow –6.987	11.4	—	3	–5.927 \Leftrightarrow –0.193
	26.027–26.045	–5.945 \Leftrightarrow –5.927	11.5 ∇	± 0.1	3	
	Oct. 1.779–1.783	–0.193 \Leftrightarrow –0.189	11.1	—	3	
	3.990–4.005	+2.018 \Leftrightarrow +2.033	11.2	—	3	
	4.923–4.928	+2.951 \Leftrightarrow +2.956	11.3	—	3	
7.864–7.869	+5.892 \Leftrightarrow +5.897	11.3	0.1	3		
I72	Sept. 26.892–26.898	–5.080 \Leftrightarrow –5.074	11.5 ∇	± 0.1	3	–5.074 \Leftrightarrow –0.124
	Oct. 1.848–1.854	–0.124 \Leftrightarrow –0.118	11.1	—	3	
	4.919–4.923	+2.947 \Leftrightarrow +2.951	11.3	—	3	
	5.968–5.971	+3.996 \Leftrightarrow +3.999	11.3	—	3	
	7.907–7.910	+5.935 \Leftrightarrow +5.938	11.4	—	3	
I99	Oct. 1.873–1.877	–0.099 \Leftrightarrow –0.095	11.1 ∇	± 0.1	3	< –0.099
	3.841–3.844	+1.869 \Leftrightarrow +1.872	11.1	—	3	
	4.878–4.882	+2.906 \Leftrightarrow +2.910	11.3	0.1	3	
	8.905–8.909	+6.933 \Leftrightarrow +6.937	11.4	—	3	
J01	Sept. 26.866–26.904	–5.106 \Leftrightarrow –5.068	11.7	± 0.1	3	–1.023 \Leftrightarrow +0.854
	29.957–29.979	–2.015 \Leftrightarrow –1.993	12.1	0.1	3	
	30.909–30.949	–1.063 \Leftrightarrow –1.023	11.9 ∇	0.2	3	
	Oct. 2.826–2.840	+0.854 \Leftrightarrow +0.868	11.2 ∇	—	3	
	4.815–4.847	+2.843 \Leftrightarrow +2.875	11.4	—	3	
12.949–12.955	+10.977 \Leftrightarrow +10.983	11.7	0.1	3		
J08	Sept. 24.985–25.000	–6.987 \Leftrightarrow –6.972	12.5	± 0.1	2	–1.093 \Leftrightarrow –0.058
	Oct. 1.927–1.947	–0.045 \Leftrightarrow –0.025	12.3	0.1	2	
	5.787–5.828	+3.815 \Leftrightarrow +3.856	12.3	0.1	3	
J24	Sept. 27.121–27.125	–4.851 \Leftrightarrow –4.847	11.4	± 0.1	3	–1.093 \Leftrightarrow –0.058
	29.150–29.162	–2.822 \Leftrightarrow –2.810	11.2	—	3	
	Oct. 6.011–6.018	+4.039 \Leftrightarrow +4.046	11.1	—	3	
	7.018–7.033	+5.046 \Leftrightarrow +5.061	11.0	—	3	
J38	Sept. 30.875–30.879	–1.097 \Leftrightarrow –1.093	11.4 ∇	—	3	–1.093 \Leftrightarrow –0.058
	Oct. 1.914–1.916	–0.058 \Leftrightarrow –0.056	11.1	—	3	
	4.948–4.950	+2.976 \Leftrightarrow +2.978	11.3	—	3	
	5.910–5.913	+3.938 \Leftrightarrow +3.941	11.3	—	3	
	8.969–8.971	+6.997 \Leftrightarrow +6.999	11.5	—	3	

The data from the eight sites that did constrain the onset of outburst III from both sides were also used to compute the average magnitude jump in this event, which was found to be 0.5 ± 0.2 magnitude. As a fair lower limit to the event's amplitude, this value suggests that the October 1 flare-up was probably barely what was accepted in Sec. 2 as a minimum brightening that still deserves to be called an outburst (an amplitude of 0.8–1.0 magnitude). If so, it is nothing short of remarkable that the method of nuclear magnitudes turned out to be as successful in detecting outburst III as the above account demonstrates.

The continuing search along the near-perihelion orbital arc in a massive data set starting in early October, several days after the onset time of outburst III, revealed no further explosive events. Thus, one of the primary tasks of this investigation has been completed.

For the data from the post-outburst period of comet 168P in Table 5, the listed six columns are identical to the first six columns in Tables 2–4. In the absence of further outbursts, the seventh column is not in Table 5 needed. Out of the total of 34 observing sites included in Table 5, the nuclear magnitudes from 18 — 213, 215, 945, 954, A24, B50, B53, B59, B70, B96, C36, C47, G26, I57, I72, I88, J01, and J24 — show, within the errors involved, no clear sign of deviation from an essentially continuous, even though somewhat uneven, brightness decrease with time during the entire period from the first week of October until December 11, when this study of the comet's activity is terminated. On the other hand, the data from the 16 remaining sites do show one or more instances of temporally localized brightening. These potential events are marked in Table 5 by wedges with a question mark. The existence of some of them appears to be supported by the data from more than one site. Fully 13 of the 16 sites — 510, 958, A71, A77, C10, C23, C90, H06, H47, I79, I99, J38, and J47 — show at least one episode of brightening in the broad time span between October 21 and November 7. Two of these sites suggest more such episodes: site 958 implies two pairs of them, the first pair between October 23 and 27 and between October 27 and 28, the second pair between November 3 and 5 and between November 5 and 6. Site A77 indicates two episodes, one between October 23 and 29 and the second between October 29 and November 2. Yet, the data from sites 213, 215, 850, 945, B50, B59, B70, B96, C36, C86, H45, I57, I72, I88, and J01, which cover this time span or parts of it, show that, within the errors of measurement, the comet's nuclear brightness was during the two weeks either nearly steady or somewhat subsiding.

The only other instances of brightening detected in the nuclear magnitudes from more than one observing site in Table 5 are found in mid-November: between November 13 and 15 from site H47, between November 14 and 17 from site 958, and between November 17 and 18 from site H45. Nominally, this looks like a pair of events: the constraint from site 958 is consistent with that from site H47 or H45, but the constraints from H47 and H45 do not refer to the same event. Again, no brightening in this general range of time is apparent in the data from sites 213, 945, B59, C23, C86, G26, I57, I72, I79, I88, J01, and J38. Only isolated instances of brightening are suggested by the data from single sites: between October 10 and 11 from site 850, between October 15 and 16,

between November 11 and 12, and between December 7 and 11 from site 958, and, finally, between December 3 and 7 from site C86.

Because the second of the two required conditions near the end of Sec. 2.2 is not satisfied, the above account of the suspected cases of brief brightening in Table 5 provides no evidence on outbursts after October 1. These instances could perhaps be explained either as very brief minor fluctuations of near-nucleus activity or as due to instrumental/data-reduction problems, including a possible interference by a field star or stars, whose contribution was not properly removed from the measured signal. The broad event between late October and early November likewise cannot be an outburst because of the enormous incompatibility of the data from different observing sites. Its true nature cannot readily be established from mere inspection of Table 5, and a different approach is implemented below. Toward that end, I next comment on the factors that determine the measured nuclear magnitudes published by the MPC and then assess the usefulness of these data beyond their initially recognized role as discriminators in the applied method for determining the outbursts' onset time.

3.2. More Information from the Nuclear Magnitudes

The general feeling of perplexity surrounding the physical meaning and use of the nuclear magnitudes of comets presented in the *Minor Planet Circulars* and the *Minor Planet Electronic Circulars* (Sec. 2.2) stems primarily from the uncertainty as to what volume of the inner coma do they refer to. The nuclear magnitude of a comet's inner coma (or nuclear condensation) measured within a circular aperture centered in a CCD image on the nucleus describes an amount of radiation coming from a cylindrical volume of space whose diameter at the nucleus depends — besides the technical characteristics of the CCD sensor — on: (1) the comet's geocentric distance, (2) the focal distance of the telescope used, (3) the wavelength-dependent sensitivity of the telescope setup (color filter used with the CCD chip), (4) the pixel scale, and (5) the chosen pixel size of the sampling aperture by the person who reduces the imaging data.

Unfortunately, the format of the MPC astrometric reports of comets does not provide information included in points (1) and (3) through (5). While the geocentric distance can readily be computed from an ephemeris, the facts in the other three points cannot be recovered and are lost. Even worse, for the observing sites with multiple instrumentation the report format fails to indicate which observations were made with which telescope.

There are only two pieces of information that can be invoked to get at least a crude idea on the volume of space sampled by the nuclear magnitudes. One, in the *Guide to Minor Body Astrometry*⁷ it is recommended that the pixel scale not exceed, preferably, $2''/\text{pixel}$ or, at worst, $3''/\text{pixel}$, while simultaneously maintaining a high enough signal-to-noise ratio. And, two, in an attempt to standardize the procedure at least to some extent, the use of an aperture $10''$ in radius was proposed by

⁷ See the information web site of the *IAU Minor Planet Center* <http://www.minorplanetcenter.net/iau/info/Astrometry.html>. A detailed description of the issues related to CCD astrometry and photometry of comets is given in Green (1997a, 1997b).

Table 5. Fading of nuclear condensation of comet 168P after outburst III (until December 11, 2012).

Site code	Observation times t_{obs} (2012 UT)	Range of times $t_{\text{obs}} - t_{\pi}$ (days)	$\langle H_N \rangle$ (mag)	RMS (mag)	No. obs.	Site code	Observation times t_{obs} (2012 UT)	Range of times $t_{\text{obs}} - t_{\pi}$ (days)	$\langle H_N \rangle$ (mag)	RMS (mag)	No. obs.	
213	Oct. 7.909–7.910	+5.937 \Leftrightarrow +5.938	11.4	—	2	958 (cont.)	Nov. 7.787–7.824	+36.815 \Leftrightarrow +36.852	13.8	± 0.1	4	
	8.916–8.926	+6.944 \Leftrightarrow +6.954	11.5	± 0.1	3		11.922–11.941	+40.950 \Leftrightarrow +40.969	14.4	0.1	3	
	11.918–11.923	+9.946 \Leftrightarrow +9.951	11.6	—	3		12.849–12.874	+41.877 \Leftrightarrow +41.902	14.0	0.1	3	
	13.830–13.907	+11.858 \Leftrightarrow +11.935	12.1	—	3		13.833–13.857	+42.861 \Leftrightarrow +42.885	14.5	0.1	3	
	16.837–16.871	+14.865 \Leftrightarrow +14.899	12.8	0.1	3		14.788–14.825	+43.816 \Leftrightarrow +43.853	14.7	0.1	4	
	24.795–24.806	+22.823 \Leftrightarrow +22.834	13.3	0.1	3		17.794–17.827	+46.822 \Leftrightarrow +46.855	14.2	0.1	4	
	27.915–27.942	+25.943 \Leftrightarrow +27.970	13.2	—	3		18.937–18.961	+47.965 \Leftrightarrow +47.989	15.1	0.1	3	
	28.804–28.828	+26.832 \Leftrightarrow +26.856	13.1	—	3		19.786–19.822	+48.814 \Leftrightarrow +48.850	15.3	0.1	4	
	Nov. 3.804–3.811	+32.832 \Leftrightarrow +32.839	13.5	0.1	3		21.947–21.970	+50.975 \Leftrightarrow +50.998	14.9	0.2	3	
	10.733–10.774	+39.761 \Leftrightarrow +39.802	13.9	0.1	3		22.741–22.765	+51.769 \Leftrightarrow +51.793	15.3	0.1	3	
	11.873–11.883	+40.901 \Leftrightarrow +40.911	13.9	—	3		24.775–24.811	+53.803 \Leftrightarrow +53.839	16.0	0.1	3	
	15.840–15.871	+44.868 \Leftrightarrow +44.899	14.5	0.1	3		28.754–28.857	+57.782 \Leftrightarrow +57.885	16.4	0.1	4	
	20.874–20.882	+49.902 \Leftrightarrow +49.910	15.0	—	3		29.869–29.894	+58.897 \Leftrightarrow +58.922	16.1	0.1	3	
Dec.	30.773–30.781	+59.801 \Leftrightarrow +59.809	15.9	0.1	3	30.771–30.807	+59.799 \Leftrightarrow +59.835	16.2	0.1	4		
	1.763–1.780	+60.791 \Leftrightarrow +60.808	15.9	0.1	3	Dec. 6.847–6.859	+65.875 \Leftrightarrow +65.887	16.7	0.1	2		
	4.847–4.854	+63.875 \Leftrightarrow +63.882	16.0	0.1	3	7.864–7.907	+66.892 \Leftrightarrow +66.935	16.8	0.1	3		
215	Oct. 19.791–19.792	+17.819 \Leftrightarrow +17.820	14.0	± 0.1	2	11.771–11.788	+70.799 \Leftrightarrow +70.816	16.4	—	2		
	25.778–25.782	+23.806 \Leftrightarrow +23.810	13.9	0.4	3	A24	Dec. 3.821–3.866	+62.849 \Leftrightarrow +62.894	16.8	± 0.1	3	
	Nov. 6.741–6.745	+35.769 \Leftrightarrow +35.773	13.3	0.2	6		4.900–4.922	+63.928 \Leftrightarrow +63.950	17.1	0.2	4	
15.768–15.770	+44.796 \Leftrightarrow +44.798	14.1	0.1	3	5.779–5.826		+64.807 \Leftrightarrow +64.854	17.0	0.1	4		
510	Oct. 16.974–17.008	+15.002 \Leftrightarrow +15.036	13.9	$\pm 0.0_4$	5	9.796–9.797	+68.824 \Leftrightarrow +68.825	17.3	0.1	2		
	19.890–19.916	+17.918 \Leftrightarrow +17.944	14.5	0.1	4	9.921–9.972	+68.949 \Leftrightarrow +69.000	17.4	0.3	4		
	28.726–28.769	+26.754 \Leftrightarrow +26.797	14.4	0.1	4	10.960–10.961	+69.988 \Leftrightarrow +69.989	16.9	0.6	2		
	31.779–31.794	+29.807 \Leftrightarrow +29.822	14.0	0.0 ₄	5	11.873–11.874	+70.901 \Leftrightarrow +70.902	16.6	—	2		
850	Oct. 9.143–9.173	+7.171 \Leftrightarrow +7.201	12.5	± 0.1	3	11.939–11.940	+70.967 \Leftrightarrow +70.968	17.0	0.4	2		
	10.138–10.212	+8.166 \Leftrightarrow +8.240	12.5	0.1	6	A71	Oct. 16.912–16.915	+14.940 \Leftrightarrow +14.943	14.2	± 0.1	5	
	11.092–11.122	+9.120 \Leftrightarrow +9.150	11.6	0.4	3		20.939–20.944	+18.967 \Leftrightarrow +18.972	14.5	0.1	5	
	21.143–21.297	+19.171 \Leftrightarrow +19.325	13.0	0.5	7	Nov. 2.750–2.763	+31.778 \Leftrightarrow +31.791	13.3	0.3	5		
	22.163–22.197	+20.191 \Leftrightarrow +20.225	13.6	0.5	3	17.882–17.896	+46.910 \Leftrightarrow +46.924	14.9	0.5	6		
	23.138–23.199	+21.165 \Leftrightarrow +21.227	13.9	0.1	5	A77	Oct. 15.761–15.772	+13.789 \Leftrightarrow +13.800	11.1	—	3	
	24.254–24.314	+22.282 \Leftrightarrow +22.342	13.5	0.5	5		23.750–23.754	+21.778 \Leftrightarrow +21.782	14.0	± 0.1	3	
	25.174–25.284	+23.202 \Leftrightarrow +23.312	12.9	0.1	6	29.814–29.839	+27.842 \Leftrightarrow +27.867	13.5	0.1	3		
Nov. 14.189–14.298	+43.217 \Leftrightarrow +43.326	14.4	0.4	6	Nov. 2.719–2.731	+31.747 \Leftrightarrow +31.759	12.4	0.1	3			
945	Oct. 5.073–5.095	+3.101 \Leftrightarrow +3.123	11.3	—	5	B50	Oct. 11.876–11.897	+9.904 \Leftrightarrow +9.925	12.5	± 0.2	4	
	8.880–8.892	+6.908 \Leftrightarrow +6.920	11.4	—	5		12.946–12.971	+10.974 \Leftrightarrow +10.999	12.5	0.1	4	
	19.890–19.908	+17.918 \Leftrightarrow +17.936	13.2	± 0.1	5		15.859–15.870	+13.887 \Leftrightarrow +13.898	12.9	0.1	3	
	20.966–20.983	+18.994 \Leftrightarrow +19.011	13.1	0.0 ₄	5	16.920–16.932	+14.948 \Leftrightarrow +14.960	13.4	0.3	2		
	21.917–21.936	+19.945 \Leftrightarrow +19.964	13.2	0.0 ₄	5	17.827–17.860	+15.855 \Leftrightarrow +15.888	14.0	0.1	3		
	25.909–25.932	+23.937 \Leftrightarrow +23.960	13.2	—	5	Nov. 18.866–18.866	+47.894 \Leftrightarrow +47.894	14.4	—	1		
	29.009–29.034	+27.037 \Leftrightarrow +27.062	13.0	—	5	B53	Oct. 5.912–5.925	+3.940 \Leftrightarrow +3.953	12.6	—	6	
	30.963–30.986	+28.991 \Leftrightarrow +29.014	13.1	—	5		19.877–19.895	+17.905 \Leftrightarrow +17.923	13.5	± 0.1	8	
	Nov. 4.938–4.967	+33.966 \Leftrightarrow +33.995	13.3	—	5		20.880–20.910	+18.908 \Leftrightarrow +18.938	13.4	0.1	8	
	12.935–12.960	+41.963 \Leftrightarrow +41.988	14.0	0.1	5	20.949–20.969	+18.977 \Leftrightarrow +18.997	13.6	0.0 ₄	10		
14.015–14.042	+43.043 \Leftrightarrow +43.070	14.0	—	5	Dec. 3.766–3.790	+62.794 \Leftrightarrow +62.818	16.7	0.3	10			
21.892–21.924	+50.920 \Leftrightarrow +50.952	15.0	0.1	5	B59	Oct. 21.799–21.806	+19.827 \Leftrightarrow +19.834	14.0	± 0.1	5		
954	Oct. 4.875–4.910	+2.903 \Leftrightarrow +2.938	11.6	± 0.4		2	28.810–28.821	+26.838 \Leftrightarrow +26.849	14.4	0.1	4	
	5.001–5.036	+3.029 \Leftrightarrow +3.064	11.7	0.2		2	31.846–31.859	+29.874 \Leftrightarrow +29.887	14.6	0.2	6	
	6.848–7.214	+4.876 \Leftrightarrow +5.242	11.6	0.1	3	Nov. 12.779–12.790	+41.807 \Leftrightarrow +41.818	13.9	0.5	4		
	9.905–9.905	+7.933 \Leftrightarrow +7.933	12.1	—	1	16.759–16.767	+45.787 \Leftrightarrow +45.795	15.1	0.5	4		
	12.108–12.205	+10.136 \Leftrightarrow +10.233	11.9	0.1	3	B70	Oct. 15.911–15.919	+13.939 \Leftrightarrow +13.947	12.7	± 0.2	3	
958	Oct. 7.909–7.939	+5.937 \Leftrightarrow +5.967	11.0	± 0.1	4		28.764–28.787	+26.792 \Leftrightarrow +26.815	13.7	0.2	3	
	9.065–9.096	+7.093 \Leftrightarrow +7.124	11.5	0.1	3	Nov. 1.847–1.933	+30.875 \Leftrightarrow +30.961	14.0	0.1	3		
	9.889–9.972	+7.917 \Leftrightarrow +8.000	11.4	0.1	7	Dec. 4.809–4.843	+63.837 \Leftrightarrow +63.871	17.2	0.3	2		
	11.007–11.033	+9.035 \Leftrightarrow +9.061	11.5	0.1	6	B96	Oct. 10.972–10.993	+9.000 \Leftrightarrow +9.021	11.6	± 0.6	14	
	15.922–15.951	+13.950 \Leftrightarrow +13.979	12.5	0.1	4		11.001–11.012	+9.029 \Leftrightarrow +9.040	13.0	0.1	8	
	16.864–16.909	+14.892 \Leftrightarrow +14.937	11.7	0.1	3		22.882–22.905	+20.910 \Leftrightarrow +20.933	14.9	0.1	12	
	22.856–22.886	+20.884 \Leftrightarrow +20.914	13.4	0.1	4		27.910–27.932	+25.948 \Leftrightarrow +25.960	14.2	0.5	13	
	23.909–23.938	+21.937 \Leftrightarrow +21.966	14.2	0.1	4		Nov. 1.753–1.771	+30.781 \Leftrightarrow +30.799	14.3	0.2	7	
	27.895–27.934	+25.923 \Leftrightarrow +25.962	13.3	0.1	4		2.808–2.831	+31.836 \Leftrightarrow +31.859	14.5	0.1	13	
	28.902–28.949	+26.930 \Leftrightarrow +26.977	12.8	0.0 ₄	5		2.869–2.884	+31.897 \Leftrightarrow +31.912	14.6	0.1	9	
	29.847–29.879	+27.875 \Leftrightarrow +27.907	13.0	0.1	5		14.789–14.808	+43.817 \Leftrightarrow +43.836	14.8	0.1	10	
	30.888–30.918	+28.916 \Leftrightarrow +28.946	12.9	0.1	4		C10	Oct. 5.949–5.970	+3.977 \Leftrightarrow +3.998	11.1	—	4
	31.850–31.882	+29.878 \Leftrightarrow +29.910	13.7	0.1	5			22.792–22.814	+20.820 \Leftrightarrow +20.842	13.3	—	4
	Nov. 3.923–3.950	+32.951 \Leftrightarrow +32.978	14.0	0.1	3	27.817–27.909		+25.845 \Leftrightarrow +25.937	12.9	$\pm 0.0_4$	13	
4.931–5.054	+33.959 \Leftrightarrow +34.082	13.5	0.1	3	Nov. 4.781–4.825	+33.809 \Leftrightarrow +33.853	13.2	0.1	4			
5.850–5.887	+34.878 \Leftrightarrow +34.915	13.8	0.1	3	30.723–30.751	+59.751 \Leftrightarrow +59.779	15.5	0.1	5			
6.847–6.877	+35.875 \Leftrightarrow +35.905	13.0	0.1	4								

Table 5 (continued).

Site code	Observation times t_{obs} (2012 UT)	Range of times $t_{\text{obs}} - t_{\pi}$ (days)	$\langle H_N \rangle$ (mag)	RMS (mag)	No. obs.	Site code	Observation times t_{obs} (2012 UT)	Range of times $t_{\text{obs}} - t_{\pi}$ (days)	$\langle H_N \rangle$ (mag)	RMS (mag)	No. obs.	
C23	Oct. 9.860–9.891	+7.888 \Leftrightarrow +7.919	11.7	± 0.2	3	H47	Oct. 19.171–19.195	+17.199 \Leftrightarrow +17.223	13.6	± 0.1	3	
	10.919–10.962	+8.947 \Leftrightarrow +8.990	11.7	0.3	3		23.115–23.179	+21.143 \Leftrightarrow +21.207	14.3	0.1	4	
	16.898–16.907	+14.926 \Leftrightarrow +14.935	12.3	0.5	3		Nov. 7.073–7.096	+36.101 \Leftrightarrow +36.124	13.1	0.1	3	
	21.826–21.842	+19.854 \Leftrightarrow +19.870	12.8	—	3		8.063–8.110	+37.091 \Leftrightarrow +37.138	13.5	0.4	4	
	22.904–22.926	+20.932 \Leftrightarrow +20.954	13.4	0.5	3		10.109–10.137	+39.137 \Leftrightarrow +39.165	14.3	0.1	4	
	27.055–27.097	+25.083 \Leftrightarrow +25.125	13.0	0.1	3		13.058–13.079	+42.086 \Leftrightarrow +42.107	14.4	0.1	3	
	27.855–27.873	+25.883 \Leftrightarrow +25.901	13.0	0.1	3		15.079–15.107	+44.107 \Leftrightarrow +44.135	13.9	0.1	3	
	28.738–28.766	+26.766 \Leftrightarrow +26.794	13.9	0.2	3		17.075–17.109	+46.103 \Leftrightarrow +46.137	14.2	0.1	7	
	31.729–31.756	+29.757 \Leftrightarrow +29.784	12.9	0.1	3		25.055–25.064	+54.083 \Leftrightarrow +54.092	15.0	0.1	3	
	Nov. 2.799–2.825	+31.827 \Leftrightarrow +31.853	13.1	0.1	3		26.103–26.109	+55.131 \Leftrightarrow +55.137	16.3	0.3	2	
	5.805–5.816	+34.833 \Leftrightarrow +34.844	13.2	0.2	3		29.093–29.100	+58.121 \Leftrightarrow +58.128	16.4	0.3	3	
	10.753–10.780	+39.781 \Leftrightarrow +39.808	13.6	0.2	3		30.063–30.091	+59.091 \Leftrightarrow +59.119	16.3	0.2	3	
	14.766–14.789	+43.794 \Leftrightarrow +43.817	13.6	0.2	3		Dec. 1.071–1.090	+60.099 \Leftrightarrow +60.118	16.2	—	3	
	20.979–20.996	+50.007 \Leftrightarrow +50.024	14.6	0.6	3		2.058–2.078	+61.086 \Leftrightarrow +61.106	16.0	0.5	4	
	25.915–25.927	+54.943 \Leftrightarrow +54.955	14.9	0.2	3		3.067–3.083	+62.095 \Leftrightarrow +62.111	16.1	0.5	5	
Dec. 8.736–8.744	+67.764 \Leftrightarrow +67.772	16.1	0.2	3	11.040–11.059	+70.068 \Leftrightarrow +70.087	17.5	0.4	2			
10.977–10.991	+70.005 \Leftrightarrow +70.019	16.0	0.6	3	I57	Oct. 7.864–7.869	+5.892 \Leftrightarrow +5.897	11.3	± 0.1	3		
C36	Oct. 5.817–5.833	+3.845 \Leftrightarrow +3.861	10.3	± 0.2		11	8.997–9.007	+7.025 \Leftrightarrow +7.035	11.5	—	3	
	11.709–11.719	+9.737 \Leftrightarrow +9.747	10.5	0.1		9	9.889–9.902	+7.917 \Leftrightarrow +7.930	11.7	0.1	3	
	12.824–12.833	+10.852 \Leftrightarrow +10.861	10.5	0.1		7	14.052–14.054	+12.080 \Leftrightarrow +12.082	12.1	0.1	3	
	13.763–13.768	+11.791 \Leftrightarrow +11.796	10.6	—		3	22.893–22.896	+20.921 \Leftrightarrow +20.924	13.4	—	3	
	26.754–26.769	+24.782 \Leftrightarrow +24.797	12.9	0.4		8	Nov. 7.987–8.007	+37.015 \Leftrightarrow +37.035	13.6	0.1	3	
	Nov. 1.743–1.752	+30.771 \Leftrightarrow +30.780	12.8	0.1		8	8.815–8.819	+37.843 \Leftrightarrow +37.847	13.7	—	3	
C47	Oct. 13.972–13.986	+12.000 \Leftrightarrow +12.014	13.3	± 0.2		7	9.904–9.908	+38.932 \Leftrightarrow +38.936	13.7	—	3	
	19.878–19.895	+17.906 \Leftrightarrow +17.923	14.9	0.6		6	10.888–10.897	+39.916 \Leftrightarrow +39.925	13.8	—	3	
	20.766–20.783	+18.794 \Leftrightarrow +18.811	14.6	0.4		6	12.938–12.978	+41.966 \Leftrightarrow +42.006	14.1	—	3	
	Nov. 2.759–2.770	+31.787 \Leftrightarrow +31.798	14.0	0.5		4	27.934–27.939	+56.962 \Leftrightarrow +56.967	15.6	0.1	3	
C86	Oct. 15.910–15.913	+13.938 \Leftrightarrow +13.941	12.6	± 0.1		3	I72	Oct. 7.907–7.910	+5.935 \Leftrightarrow +5.938	11.4	—	3
	29.906–29.910	+27.934 \Leftrightarrow +27.938	13.2	0.1		3		13.909–13.926	+11.937 \Leftrightarrow +11.954	12.0	± 0.1	3
	Nov. 1.978–1.979	+31.006 \Leftrightarrow +31.007	13.3	—		3		15.869–15.872	+13.897 \Leftrightarrow +13.900	12.5	—	3
C90	Nov. 11.860–11.864	+40.888 \Leftrightarrow +40.892	13.9	—		3	20.988–20.992	+19.016 \Leftrightarrow +19.020	13.0	—	3	
	12.972–12.975	+42.000 \Leftrightarrow +42.003	13.7	0.1	3	27.905–27.915	+25.933 \Leftrightarrow +25.943	13.1	0.1	3		
	19.817–19.824	+48.845 \Leftrightarrow +48.852	14.8	0.1	3	28.864–28.867	+26.892 \Leftrightarrow +26.895	13.1	—	3		
	30.807–30.813	+59.835 \Leftrightarrow +59.841	15.8	0.2	3	Nov. 6.838–6.865	+35.866 \Leftrightarrow +35.893	13.4	—	3		
	Dec. 2.779–2.786	+61.807 \Leftrightarrow +61.814	15.9	—	3	11.887–11.894	+40.915 \Leftrightarrow +40.922	13.6	—	3		
	3.766–3.772	+62.794 \Leftrightarrow +62.800	16.0	0.1	3	12.843–12.849	+41.871 \Leftrightarrow +41.877	14.1	—	3		
	7.760–7.764	+66.788 \Leftrightarrow +66.792	15.1	0.1	3	19.840–19.851	+48.868 \Leftrightarrow +48.879	14.9	—	3		
	G26	Nov. 13.661–13.707	+42.689 \Leftrightarrow +42.735	14.2	± 0.04	5	22.830–22.833	+51.858 \Leftrightarrow +51.861	15.2	—	3	
		16.629–16.718	+45.657 \Leftrightarrow +45.746	14.5	0.1	5	26.917–26.959	+55.945 \Leftrightarrow +55.987	15.4	0.1	3	
		29.639–29.643	+58.667 \Leftrightarrow +58.671	15.8	0.1	2	Dec. 1.853–1.856	+60.881 \Leftrightarrow +60.884	15.6	0.1	3	
	H06	Dec. 3.524–3.565	+62.552 \Leftrightarrow +62.593	16.2	0.1	4	2.875–2.878	+61.903 \Leftrightarrow +61.906	15.9	0.1	3	
Oct. 20.235–20.243		+18.263 \Leftrightarrow +18.271	13.3	± 0.1	2	3.858–3.867	+62.886 \Leftrightarrow +62.895	15.9	—	3		
23.281–23.287		+21.309 \Leftrightarrow +21.315	13.6	—	2	I79	Oct. 23.798–23.828	+21.826 \Leftrightarrow +21.856	14.8	± 0.3	12	
23.370–23.374		+21.398 \Leftrightarrow +21.402	14.9	0.1	2		31.807–31.836	+29.835 \Leftrightarrow +29.864	13.9	0.3	11	
27.194–27.199	+25.222 \Leftrightarrow +25.227	14.6	0.1	2	Nov. 16.755–16.784		+45.783 \Leftrightarrow +45.812	15.5	0.5	11		
H45	28.309–28.322	+26.337 \Leftrightarrow +26.350	13.2	—	2	18.908–18.949	+47.936 \Leftrightarrow +47.977	16.0	0.4	11		
	29.233–29.233	+27.261 \Leftrightarrow +27.261	13.1	—	1	19.794–19.824	+48.822 \Leftrightarrow +48.852	15.9	0.5	11		
	31.276–31.292	+29.304 \Leftrightarrow +29.320	14.7	0.5	10	I88	Oct. 16.911–16.918	+14.939 \Leftrightarrow +14.946	13.6	—	3	
	Nov. 4.101–4.104	+33.129 \Leftrightarrow +33.132	14.4	—	2		Nov. 6.955–6.967	+35.983 \Leftrightarrow +35.995	13.9	—	3	
	5.217–5.229	+34.245 \Leftrightarrow +34.257	14.1	0.6	8		9.950–9.977	+38.978 \Leftrightarrow +39.005	14.2	—	3	
H45	Oct. 27.253–27.270	+25.281 \Leftrightarrow +25.298	12.1	± 0.1	10	12.985–12.990	+42.013 \Leftrightarrow +42.018	14.6	—	5		
	Nov. 4.189–4.203	+33.217 \Leftrightarrow +33.231	11.8	0.1	8	15.849–15.892	+44.877 \Leftrightarrow +44.920	15.0	—	3		
	17.241–17.251	+46.269 \Leftrightarrow +46.279	15.1	0.1	8	Dec. 2.823–2.871	+61.851 \Leftrightarrow +61.899	16.7	± 0.1	3		
	18.123–18.131	+47.151 \Leftrightarrow +47.159	14.6	0.1	7	I99	Oct. 8.905–8.909	+6.933 \Leftrightarrow +6.937	11.4	—	3	
	25.139–25.150	+54.167 \Leftrightarrow +54.178	16.4	0.1	8		9.844–9.846	+7.872 \Leftrightarrow +7.874	11.6	—	3	
	26.120–26.126	+55.148 \Leftrightarrow +55.154	16.4	0.1	6		15.856–15.861	+13.884 \Leftrightarrow +13.889	12.5	± 0.1	3	
	Dec.	28.112–28.129	+57.140 \Leftrightarrow +57.157	16.8	0.1	8	23.830–23.835	+21.858 \Leftrightarrow +21.863	13.6	—	3	
		3.080–3.111	+62.108 \Leftrightarrow +62.139	17.1	0.1	8	28.827–28.831	+26.855 \Leftrightarrow +26.859	13.0	0.1	3	
		5.108–5.116	+64.136 \Leftrightarrow +64.144	17.2	0.1	8	Nov. 12.878–12.883	+41.906 \Leftrightarrow +41.911	14.0	—	3	
		11.156–11.167	+70.184 \Leftrightarrow +70.195	17.8	0.1	8	Dec. 1.819–1.827	+60.847 \Leftrightarrow +60.855	15.8	0.1	3	
		J01	Oct. 12.949–12.955	+10.977 \Leftrightarrow +10.983	11.7	± 0.1	3	Oct. 12.949–12.955	+10.977 \Leftrightarrow +10.983	11.7	± 0.1	3
			14.904–14.913	+12.932 \Leftrightarrow +12.941	12.3	—	3	14.904–14.913	+12.932 \Leftrightarrow +12.941	12.3	—	3
20.924–20.952			+18.952 \Leftrightarrow +18.980	13.3	—	3	20.924–20.952	+18.952 \Leftrightarrow +18.980	13.3	—	3	
28.878–28.911	+26.906 \Leftrightarrow +26.939		13.2	0.1	3	28.878–28.911	+26.906 \Leftrightarrow +26.939	13.2	0.1	3		
Nov. 4.842–4.868	+33.870 \Leftrightarrow +33.896		12.9	0.3	3	Nov. 4.842–4.868	+33.870 \Leftrightarrow +33.896	12.9	0.3	3		
10.877–10.899	+39.905 \Leftrightarrow +39.927		13.3	0.4	3	10.877–10.899	+39.905 \Leftrightarrow +39.927	13.3	0.4	3		
11.852–11.885	+40.880 \Leftrightarrow +40.913	13.1	0.5	3	11.852–11.885	+40.880 \Leftrightarrow +40.913	13.1	0.5	3			

Table 5 (continued).

Site code	Observation times t_{obs} (2012 UT)	Range of times $t_{\text{obs}} - t_{\pi}$ (days)	$\langle H_N \rangle$ (mag)	RMS (mag)	No. obs.	Site code	Observation times t_{obs} (2012 UT)	Range of times $t_{\text{obs}} - t_{\pi}$ (days)	$\langle H_N \rangle$ (mag)	RMS (mag)	No. obs.
J01 (cont.)	Nov.12.833–12.899	+41.911 \Leftrightarrow +41.927	13.8	0.5	3	J38 (cont.)	Nov. 6.917–6.922	+35.945 \Leftrightarrow +35.950	13.4	—	3
	21.809–21.834	+50.837 \Leftrightarrow +50.862	15.1	0.6	3		9.947–9.954	+38.975 \Leftrightarrow +38.982	13.7	—	3
	Dec. 1.819–1.856	+60.847 \Leftrightarrow +60.884	15.9	0.1	—		13.946–13.955	+42.974 \Leftrightarrow +42.983	14.1	—	3
J24	Oct. 7.018–7.033	+5.046 \Leftrightarrow +5.061	11.0	—	3	14.909–14.919	+43.937 \Leftrightarrow +43.947	14.2	—	3	
	Nov. 9.914–9.933	+38.942 \Leftrightarrow +38.961	13.7	± 0.1	3	21.871–21.878	+50.899 \Leftrightarrow +50.906	14.9	—	3	
	Dec. 6.072–6.087	+65.100 \Leftrightarrow +65.115	15.8	0.1	3	Dec. 1.894–1.903	+60.922 \Leftrightarrow +60.931	15.8	—	3	
	6.992–6.998	+66.020 \Leftrightarrow +66.026	15.9	0.1	4	9.912–9.913	+68.940 \Leftrightarrow +68.941	16.4	—	2	
J38	Oct. 8.969–8.971	+6.997 \Leftrightarrow +6.999	11.5	—	3	J47	Oct. 5.919–5.984	+3.947 \Leftrightarrow +4.012	11.7	± 0.7	3
	16.917–16.922	+14.945 \Leftrightarrow +14.950	12.6	± 0.1	3		7.013–7.043	+5.041 \Leftrightarrow +5.071	11.2	0.1	3
	19.873–19.882	+17.901 \Leftrightarrow +17.910	13.3	0.1	3		7.065–7.081	+5.093 \Leftrightarrow +5.109	11.3	—	2
	20.873–20.876	+18.901 \Leftrightarrow +18.904	13.1	—	3		8.900–8.934	+6.928 \Leftrightarrow +6.962	11.5	—	3
	21.891–21.894	+19.919 \Leftrightarrow +19.922	13.3	—	3		23.905–23.939	+21.933 \Leftrightarrow +21.967	14.9	0.2	3
	23.892–23.896	+21.920 \Leftrightarrow +21.924	13.5	—	3		25.807–25.835	+23.835 \Leftrightarrow +23.863	13.4	$\lesssim?$	4
	25.840–25.847	+23.868 \Leftrightarrow +23.875	13.3	—	3		Nov.13.879–13.921	+42.907 \Leftrightarrow +42.949	14.6	0.7	3
	28.887–28.895	+26.915 \Leftrightarrow +26.923	13.0	$\lesssim?$	3		Dec. 2.849–2.868	+61.877 \Leftrightarrow +61.896	16.2	0.6	3
	30.977–30.986	+29.005 \Leftrightarrow +29.014	13.3	—	3		4.847–4.879	+63.875 \Leftrightarrow +63.907	16.6	1.0	3
	Nov. 4.901–4.908	+33.929 \Leftrightarrow +33.936	13.4	—	3		11.844–11.882	+70.872 \Leftrightarrow +70.910	16.9	0.9	3

Table 6. Parameters of the outbursts of comet 168P.

Outburst	Time of outburst's onset, t_{onset}		Distance (AU) from		Phase angle	Mean nuclear magnitude jump (mag)	Number of observing sites ^b	Sites whose data define t_{onset}
	Date 2012 (UT)	Δt (days) ^a	Earth	Sun				
I	Sept. 1.6 \pm 1.5	–30.4	0.494	1.456	21°	1.7 \pm 0.6	12(9)	958, C86
II	Sept. 22.64 \pm 0.29	–9.33	0.424	1.419	10	2.4 \pm 0.6	14(11)	H47, C47
III	Oct. 1.78 \pm 0.02	–0.19	0.428	1.415	12	0.5 \pm 0.2	11(8)	I57, (A77)

^a Time $\Delta t = t_{\text{onset}} - t_{\pi}$ reckoned from perihelion passage, t_{π} .

^b Number of sites that provide any constraints on t_{onset} ; number of sites with two-sided constraints is in parentheses.

Kidger (2002). As long as these two rules are followed, one finds that the inner coma of up to about 3300 km from the nucleus in the direction perpendicular to the line of sight contributed to the nuclear magnitude, when comet 168P was at geocentric distances near 0.45 AU (an average of the geocentric distances at the onset times of the three outbursts; cf. Table 6) and that the diameter of this field should be covered by 7 to 10 pixels. The median imaging scale of the telescopes listed in Table 1 is about 150"/mm, so that the preferable pixel scale is satisfied, on the average, with a pixel size of approximately 13–14 microns on a side, comparable to that of commonly available CCD arrays. However, a few instruments in Table 1 have imaging scales more than twice as large as the median, and for these even the worst acceptable pixel scale, 3"/pixel, requires CCD arrays with pixels smaller than 10 microns on a side.

Assuming conservatively that the plume of ejecta from the nucleus of comet 168P expanded at a rate of a few hundred meters per second, a very brief burst of material (unconsequential to the physical conditions at the source) released in a direction perpendicular to the line of sight should have passed through a 10" aperture in a matter of several hours at the most. Even if the direction of the plume's motion was fairly close to the line of sight, the material should have been out of the 10" aperture within one or two days, and the nuclear magnitude should then have returned to the pre-outburst level. However, if the emission event was not brief, the plume of material would have stayed within the limits of the sampling aperture longer, depending upon the event's duration.

To estimate the strength of the three outbursts, one needs to study temporal variations in the nuclear magnitudes listed in Tables 2–5. I began with site 958, which provided the most extensive data set. Abiding by the rule in Sec. 2.2 that nuclear magnitudes from different sites should not be mixed without first carefully testing them for compatibility, I compared each of the available nuclear-magnitude sets against the set from site 958, and was able to distinguish three groups of data: (A) from the sites whose nominal nuclear magnitudes turned out to be fairly consistent with those from site 958 over the entire time span, August 11–December 11, 2012, but especially before October 20; (B) from the sites whose nominal nuclear magnitudes could be made fairly consistent with those from group A during the whole time span after a constant correction has been applied to the reported nuclear magnitudes; and (C) from the sites whose nominal nuclear magnitudes could not be made consistent with the data from groups A and B without time dependent corrections. The classification is not absolute in that especially sites with large sets of observations, most (but not necessarily all) of which satisfied the rules for group A or B, were included in that group. Next to site 958, the sites in group A are 213, 945, C10, C23, C86, C90, I57, I72, I99, and J36; those in group B are 160, 215, C47, A24, D09, G26, H47, I79, I88, J24, and J38; and those in group C are 510, 585, 850, 954, A71, A77, B50, B53, B59, B70, B96, C36, H06, H45, I81, J01, J08, and J47, some of which offer the magnitudes only from October or November on (Table 5). The totals are 11 sites in group A, 11 sites in group B, and 18 sites in group C.

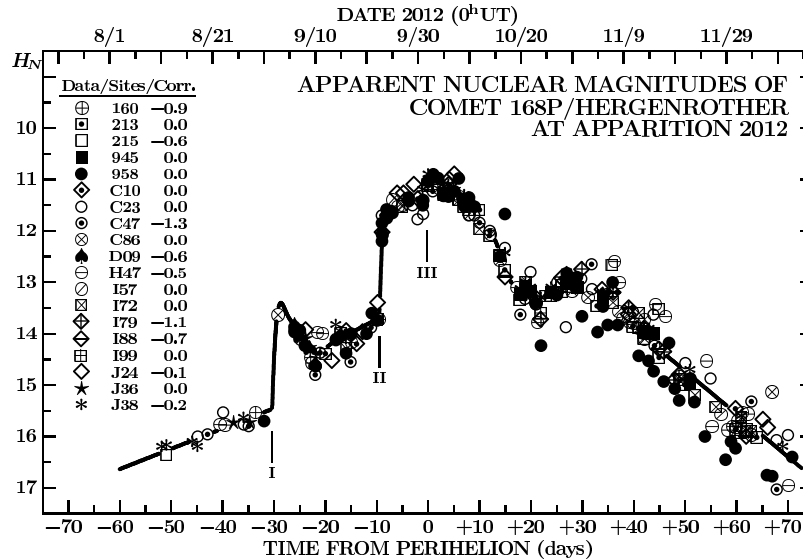


Figure 2. Temporal variations in the apparent nuclear magnitude of comet 168P/Hergenrother, derived from CCD observations obtained between August 11 and December 11, 2012, or 52 days before perihelion and 70 days after perihelion, and based on the reports from 19 sites. The data are referred to the magnitude system used at observing site 958; those from nine other sites required no corrections, while those from nine other sites were fainter and were corrected by 0.1 to 1.3 magnitudes to become comparable with the rest. The total number of plotted points is 303. The onset times of the three outbursts are identified by the roman numerals. A growing scatter among the nuclear magnitudes from different observing sites is noted toward the end of the period.

The nuclear magnitudes from most group A and group B sites are plotted against time in Figure 2, including all such magnitudes from Tables 2–4. Only the magnitudes from three such sites in Table 5, spanning short time periods, are omitted from Figure 2 (site C90 of group A and sites A24 and G26 of group B). It is clear that the restrictions on the sets of nuclear magnitudes that could be incorporated into their common light curve, while not very tight, prevent the data taken at nearly one half of all sites from being employed in Figure 2.

This figure allows one to make a number of fundamental conclusions about the near-nucleus activity of comet 168P. Outbursts I and II are prominently displayed, consistent with the large nuclear-magnitude jumps listed in Table 6. Outburst III is by no means striking, but still detectable. Figure 2 shows that the shape of the light curve in the aftermath of each of the three outbursts is quite different. The nuclear brightness is seen to have dropped rather steeply starting not later than September 5.9 UT, some 3–6 days after the onset of outburst I, suggesting that this event was a relatively brief one, with the active stage spanning hardly more than two days and possibly only a fraction of a day. However, the nuclear brightness did not return to the low-activity, pre-outburst phase, but stayed elevated by at least one magnitude until the onset of outburst II, which occurred three weeks later. Once this event commenced, practically no fading is detected in Figure 2 for about 7 days, so outburst II was more extended in time than outburst I. After a brief, shallow drop around September 30, the nuclear brightness began to climb again sharply on October 1, the onset of outburst III. Some sites in Table 4 indicate that this event was relatively brief, less than two days, while others suggest that the brightness plateau extended over as many as five days. On the average, the comet’s activity surely began to subside by October 9.

From Figure 2, the approximate amplitude is 1.9 magnitudes for outburst I, 2.6 magnitudes for outburst II, and not more than 0.8 magnitude for outburst III. These amplitudes are clearly correlated with the average magnitude jumps in Table 6, exceeding them by 0.2 to 0.3 magnitude, but they are not directly related to the amount and mass of the material ejected in each event because the magnitude scale is logarithmic. In arbitrary brightness units, the estimated amplitudes correspond to the peak rates of surge in a ratio of 2, 20, and 15, respectively, for the three events. Thus, outburst II was the most powerful one in terms of both the peak brightness surge and the duration.

As for the category of the outbursts, I have been unable to find any information on changes in the gas-to-dust ratio potentially associated with outburst I. Only incomplete data are currently available for comet 168P on temporal variations in the product $Af\rho$, introduced by A’Hearn et al. (1984) as a proxy to measure the abundance of dust in the coma. Sostero et al. (2012) calculated $Af\rho$ to equal 670 cm on September 26.6 UT, 1210 cm on October 3.6 UT, and 850 cm on October 9.6 UT within about 3000 km of the nucleus on CCD images (plus a red filter) taken with the 200-cm $f/10$ Ritchey-Chrétien Faulkes-South reflector at Siding Spring. An expanded sample of $Af\rho$ values by G. Sostero, G. Milani, and E. Bryssinck, referring to a circular aperture of 10,000 km in radius at the comet, is available on the *comets-ml* website.⁸ Although this graph contains about 30 data points, only five of them are in the relevant 30-day window between the beginning of September and early October. On September 12 and 14, about midway between outbursts I and II, as well as on September 22.0 UT, shortly before the onset of outburst II, $Af\rho$ was

⁸ At <http://tech.groups.yahoo.com/group/comets-ml>, message number 20108, date November 6, 2012.

merely 50 cm,⁹ increasing to 350 ± 70 cm on September 26, four days after the onset of outburst II, and to the rather impressive 1500 ± 300 cm on September 28, three days before the onset of outburst III. Five days later, on October 3, $Af\rho$ dropped back to 740 ± 150 cm and its nominal value in Sostero et al.’s plot, which extends to early November, never exceeded 700 cm after October 5 and 200 cm after October 20. Finally, in an account of his photometric observations on October 9, Schleicher (2012) gives $Af\rho \simeq 300$ cm, about a factor of two smaller than the value shown by Sostero et al. on their plot. These numbers can be compared with the comet’s spectrum by C. Buil, who, also on October 9, reported a strong continuum, with only a CN band at 3883 Å and faint [O I] lines at 5577 Å and 6300 Å being detected.¹⁰

Based on all this evidence, outbursts II and III appear to have been dust dominated events. Although no relevant information is available for outburst I, it is probably rather safe to speculate that it too was dominated by dust.

Figure 2 also provides information on the shape of the broad event in late October and early November. Clearly the fairly rapid drop in the near-nucleus activity that followed outburst III ceased on or around October 21 and in the following two or so weeks the nuclear brightness either stagnated or even surged up a little, suggesting possibly a limited re-activation of the nucleus. The data from the various observing sites do not provide a consistent answer as to what exactly was happening, but the event certainly was not a major flare-up. After November 7 the fairly steep rate of brightness decrease generally resumed, continuing until the end of the investigated period of time, 70 days after perihelion.

4. FRAGMENTATION OF COMET 168P/HERGENROTHER AND A CORRELATION OF THE SEPARATION TIMES WITH THE ONSET TIMES OF THE OUTBURSTS

The first report of a secondary nucleus came from Sostero et al. (2012) who detected it on stacked images taken with the 200-cm f/10 Ritchey-Chrétien Faulkes-North reflector atop Haleakala, Maui, on October 26.4 UT. This fragment B was located about $2''$ south and slightly to the west of the primary nuclear condensation (now fragment A), was of magnitude ~ 17 , and had a diffuse coma nearly $2''$ in diameter. Fragment B was still visible on images taken with the same telescope on November 2 and 3, but not on November 7, when it must have been fainter than magnitude 20. However, on this last date Sostero et al. suspected another extremely faint fragment a little more than $8''$ to the southeast from the primary, which however was not confirmed.¹¹

Stevenson et al. (2012) reported the results of their observations of comet 168P with the 810-cm Gemini-North telescope atop Mauna Kea, Hawaii, on October 28 and November 2. On both nights they confirmed the presence of fragment B and on the second night they detected two

additional fragments, C about $6''$ to the southeast of the primary and D more than $11''$ to the south-southeast of the primary.

Hergenrother (2012a, 2012b) measured a total of five nuclear companions in a number of the comet’s images taken with the Faulkes-North reflector on October 26 and November 2–3 and by Y. Fernandez and E. Kramer with the 210-cm telescope atop Kitt Peak between November 2 and 12. The details of all measurements of companions B–G employed in the present investigation are listed in Table 7, which also includes privately communicated information from Hergenrother on his unpublished measurement of companion D in the images taken with the 183-cm Vatican Advanced Technology Telescope atop Mount Graham on November 17.

4.1. Determining the Fragmentation Parameters

The motions of the six companions of comet 168P are now modeled to derive the fragmentation parameters, employing the technique developed by the author more than three decades ago (Sekanina 1977, 1978, 1982) and extensively tested over the years. An upgraded version of this method, which includes the differential perturbations by the planets, was described by Sekanina and Chodas (2002).

In general, the goal is to determine up to five fragmentation parameters for a companion separating from the parent comet: the time of its breakup, called the time of separation or fragmentation, t_{frg} ; the differential deceleration γ due to outgassing; and the velocity of separation V_{sep} of the companion relative to the parent at time t_{frg} . The deceleration is assumed to act continuously in the antisolar direction and to vary as the inverse square of heliocentric distance. The right-handed RTN coordinate system is centered on the parent object, referred to its orbit plane, and defined by the orthogonal directions radial away from the Sun, transverse in the plane, and normal to the plane. The components of the separation velocity in this coordinate system are $(V_{\text{sep}})_R$ in the radial direction, $(V_{\text{sep}})_T$ in the transverse direction, and $(V_{\text{sep}})_N$ in the normal direction. The employed iterative differential-correction least-squares optimization procedure makes use of software that solves the normal equations for an arbitrary number of unknowns. The technique thus allows one to determine all five parameters [t_{frg} , γ , $(V_{\text{sep}})_R$, $(V_{\text{sep}})_T$, and $(V_{\text{sep}})_N$] or any combination of fewer than five of them; a total of 31 different versions is available. This option proves very convenient, especially in an early phase of the optimization process, before the solution “settles” near the most probable values of the parameters, or when the convergence is slow. It is also highly beneficial when a data set is too small to allow one to determine all five parameters. This feature is in the following calculations used to great advantage.

The primary task for this investigation of the motions of the six companions is to examine their implied fragmentation times and the possible correlation between them and the onset times of the three outbursts. The number of offset observations in Table 7 is very limited, so one cannot expect that the full five-parameter model could be applied, particularly because experience has shown that the derived radial component of the separation velocity, $(V_{\text{sep}})_R$, is often highly correlated with the fragmentation time t_{frg} .

⁹ This value is by a factor of 2.5 smaller than a median among the ~ 40 short-period comets in A’Hearn et al.’s (1995) sample, but much larger than the values listed for 2P/Encke, 10P/Tempel, 26P/Grigg-Skjellerup, or 45P/Honda-Mrkos-Pajdušáková.

¹⁰ Full description of Buil’s observation, made with his 23.5-cm f/10 Celestron C9 Schmidt-Cassegrain reflector, can be found at <http://www.astrosurf.com/buil/comet/hergenrother/obs.htm>.

¹¹ This fragment, if genuine, could be either companion C or F; however, neither fits quite satisfactorily.

Table 7. Offset measurements of six companions of comet 168P employed in this investigation.

Date 2012 (UT)	Separ- ation ^a	Position angle ^a	Com- panion	Measurer	Observer(s) or institution(s)	Telescope ^b	Observing site
Oct. 26.42	2'1	191'1	B	Hergenrother	Howes, Sostero, and Guido	Faulkes	Haleakala
	3.8	139.8	C	"	"	"	"
28.4	2.4	172.9	B	Stevenson	Stevenson et al. (2012)	Gemini	Mauna Kea
Nov. 2.3	2.9	162.5	B	"	"	"	"
	6.2	132.1	C	"	"	"	"
	11.4	145.1	D	"	"	"	"
2.44	3.3	167.4	B	Hergenrother	Dollar Academy/Queen's College	Faulkes	Haleakala
	5.8	133.7	C	"	"	"	"
	5.2	159.3	E	"	Fernandez & Kramer ^c	210-cm refl.	Kitt Peak
3.28	3.1	165.3	B	"	Maui Community College	Faulkes	Haleakala
	6.4	131.7	C	"	"	"	"
	5.0	151.0	E	"	Fernandez & Kramer ^c	210-cm refl.	Kitt Peak
6.28	3.3	160.9	B	"	"	"	"
	9.1	148.3	F	"	"	"	"
6.30	3.6	164.8	B	"	"	"	"
	9.3	149.1	F	"	"	"	"
7.30	3.6	162.4	B	"	"	"	"
7.31	6.0	159.1	E	"	"	"	"
	9.5	143.9	F	"	"	"	"
7.32	3.5	165.6	B	"	"	"	"
8.27	5.7	164.0	E	"	"	"	"
8.29	5.7	165.3	E	"	"	"	"
11.35	9.7	168.0	G	"	"	"	"
12.29	9.8	163.9	G	"	"	"	"
17.30	14.1	151.4	D	"	Hergenrother	VATT	Mt. Graham

^a Angular distance from the nuclear condensation of the primary component and the position angle measured from north through east.

^b Abbreviations: Faulkes = 200-cm Faulkes-North reflector; Gemini = 810-cm Gemini-North reflector; VATT = 183-cm Vatican Advanced Technology Telescope.

^c Image made available by B. E. A. Mueller.

In an effort to find the best possible fragmentation parameters, I search for different solutions to the available data set of each companion. To mark them apart, I assign each solution a group of letters, which indicate what parameters are included; F stands for the fragmentation time, D for the deceleration, and R, T, and N for the radial, transverse, and normal components of the separation velocity, respectively. Thus, for example, solution FD means that only the fragmentation time and the deceleration are solved for and that the separation velocity is forced to be zero; similarly, solution DRN means that the deceleration and the radial and normal components of the separation velocity are solved for, with a particular forced fragmentation time and a zero transverse component of the separation velocity. Various solutions are compared in terms of the root-mean-square error and whether or not the systematic trends with time are present in the distribution of residuals “observed minus modeled” in both the right ascension [which includes the factor $\cos(\text{declination})$] and the declination. These criteria serve to assist in judging the quality of the solutions and in facilitating the final choice of the individual parameters, primarily the fragmentation time. And because the outgassing-driven deceleration has a dominant effect on the motion of any companion, the first step in the process of estimating the most probable time of fragmentation is to compute the solutions that involve these two parameters.

It should also be noted that the earth transited the orbit plane of comet 168P on September 19.2 UT, 2012, which resulted in unfavorable edge-on observing conditions in the days around this time, as any mass released from the nucleus in, or very close to, the orbit plane

was in projection onto the plane of the sky moving in the same direction. Fortunately, thanks to the comet’s 22° inclination and relatively small geocentric distance, the earth’s angular distance from the plane began to increase fairly rapidly soon after the transit, reaching 10° on September 30, 20° on October 15, and 25° by the time the first companion was detected, on October 26.

4.2. Companion B

Table 7 shows that nine measurements of the offsets of this fragment from the primary A in the images taken between October 26 and November 7 are available for computing the fragmentation parameters. Three solutions that included the fragmentation time as a variable, FD, FDT, and FDN, are listed in the first three lines of Table 8. Solution FDR and three four-parameter solutions, FDRT, FDRN, and FDTN, failed to converge.

By sheer coincidence, in the three runs, in which the fragmentation time was solved for, the computed values of this parameter just happen to span the period covered by the three outbursts, thus providing no obvious clue as to which of them is the one most probably associated with the release of this companion. However, both the comparison of solutions FD, FDT, and FDN in Table 8 and the distribution of residuals from solutions FD and FDN in Table 9 (which also shows the offsets in right ascension and declination), slightly favor a fragmentation time in the second half of September or in early October, so that outburst I is a less likely candidate. Table 9 also presents the residuals from other solutions of particular interest, based on three values of the fragmentation time forced to coincide with the onset time of each of the three outbursts. Solutions DN and DRN appear to

Table 8. Fragmentation solutions for companions B–G of comet 168P.

Companion	Number of data points	Solution	Time of fragmentation ^a 2012 (UT)	Differential deceleration (units ^b)	Components of separation velocity (m/s)			Mean residual
					(V_{sep}) _R	(V_{sep}) _T	(V_{sep}) _N	
B	9	FD	Sept. 1.7 ± 2.7	5.41 ± 0.59	$\pm 0''.29$
		FDT	Oct. 2.1 ± 4.2	20.6 ± 5.1	-0.22 ± 0.06	± 0.20
		FDN	Sept. 17.5 ± 2.5	15.0 ± 2.9	$+0.18 \pm 0.05$	± 0.20
		DT	(Sept. 1.60)	5.37 ± 0.18	0.00 ± 0.01	± 0.29
		DT	(Sept. 22.64)	12.47 ± 0.33	-0.12 ± 0.01	± 0.22
		DT	(Oct. 1.78)	20.23 ± 0.50	-0.21 ± 0.01	± 0.20
		DN	(Sept. 1.60)	5.58 ± 0.26	$+0.01 \pm 0.01$	± 0.28
		DN	(Sept. 22.64)	22.6 ± 0.9	$+0.31 \pm 0.03$	± 0.23
		DN	(Oct. 1.78)	52.4 ± 5.3	$+0.72 \pm 0.12$	± 0.56
		DRN	(Sept. 1.60)	12.3 ± 1.7	-0.32 ± 0.08	$+0.13 \pm 0.03$	± 0.21
		DRN	(Sept. 22.64)	15.8 ± 3.1	$+0.20 \pm 0.09$	$+0.22 \pm 0.04$	± 0.21
		DRN	(Oct. 1.78)	14.9 ± 4.7	$+0.91 \pm 0.10$	$+0.38 \pm 0.06$	± 0.23
		DTN	(Sept. 1.60)	9.4 ± 1.1	$+0.15 \pm 0.04$	$+0.22 \pm 0.06$	± 0.22
		DTN	(Sept. 22.64)	17.1 ± 2.3	-0.07 ± 0.03	$+0.14 \pm 0.07$	± 0.20
DTN	(Oct. 1.78)	21.5 ± 3.5	-0.21 ± 0.02	$+0.03 \pm 0.08$	± 0.20		
C	4	FD	Oct. 8.0 ± 1.4	79 ± 9	± 0.32
		FDT	Oct. 3.0 ± 3.9	54 ± 15	$+0.10 \pm 0.06$	± 0.28
		FDN	Oct. 7.1 ± 1.5	53 ± 12	-0.33 ± 0.14	± 0.25
		DT	(Oct. 1.78)	49.5 ± 1.1	$+0.12 \pm 0.02$	± 0.26
		DRN	(Oct. 1.78)	53 ± 11	-0.56 ± 0.21	-0.23 ± 0.12	± 0.26
D	2	FD	Sept. 19.6 ± 5.9	39 ± 11	± 1.67
		FDT	Aug. 7 ± 9	8.6 ± 2.5	$+0.57 \pm 0.05$	± 0.26
		FDN	Sept. 6 ± 10	15 ± 8	-0.49 ± 0.13	± 0.87
		DT	(Sept. 1.60)	20.0 ± 0.8	$+0.35 \pm 0.05$	± 0.74
		DN	(Sept. 1.60)	12.0 ± 1.1	-0.53 ± 0.07	± 0.66
E	5	FD	Sept. 8.7 ± 2.8	11.8 ± 1.4	± 0.43
		DT	(Sept. 1.60)	9.19 ± 0.32	$+0.05 \pm 0.02$	± 0.42
		DN	(Sept. 1.60)	7.96 ± 0.50	-0.07 ± 0.03	± 0.42
F	3	FD	Sept. 24.6 ± 1.3	40.5 ± 2.8	± 0.32
		DR	(Sept. 22.64)	40.3 ± 2.5	-0.18 ± 0.12	± 0.32
		DT	(Sept. 22.64)	36.9 ± 0.8	$+0.03 \pm 0.02$	± 0.32
		DN	(Sept. 22.64)	33.9 ± 2.0	-0.10 ± 0.07	± 0.32
G	2	FD	Aug. 29.2 ± 2.4	12.7 ± 1.0	± 0.34
		D	(Sept. 1.60)	14.23 ± 0.41	± 0.40
		DR	(Sept. 1.60)	12.6 ± 1.2	$+0.11 \pm 0.08$	± 0.34
		DT	(Sept. 1.60)	14.11 ± 0.36	-0.04 ± 0.02	± 0.34
		DN	(Sept. 1.60)	14.92 ± 0.58	$+0.05 \pm 0.04$	± 0.34

^a Forced values of fragmentation time are parenthesized.

^b Units are 10^{-5} the solar gravitational acceleration, or $0.059 \mu\text{m/s}^2$ at 1 AU from the Sun.

prefer outburst II, while solution DT favors slightly outburst III, and solution DTN is essentially inconclusive. Thus, by an extremely narrow margin, outburst II may be the most likely one to correlate with companion B. The DR-type solutions are not listed in Table 8, because they always resulted in an inferior fit, with the mean residual of about $\pm 0''.3$ or more.

4.3. Companion C

Offsets of this companion from the primary were measured only in the images from four days, between October 26 and November 3 (Table 7). The three solutions, including the fragmentation time as a variable, provide for it the dates of October 3–8 with a 1σ uncertainty of up to nearly 4 days, as shown in Table 8. The likely correlation with outburst III is supported by the two solutions, DT and DRN, that were run on the assumption that the release of companion C coincided with the onset of outburst III. Somewhat surprisingly, solution DTN had a somewhat larger mean residual than solution DRN and is not listed in Table 8. Judging from their mean residuals, solutions DRN and DT are both acceptable. Solution DT also offers a reasonably good distribution of residuals

in Table 10. One can conclude with some confidence that a close relationship between companion C and outburst III is quite plausible.

4.4. Companion D

This fragment was extremely faint on both November 2 and 17 and, curiously, was not detected in between the two dates. With only these two data points, one is extremely limited in terms of choice of solutions. The large gap between them also offers an opportunity for contradictory solutions that may provide an unexpectedly good fit to the two points but lead to fictitious fragmentation parameters and must be rejected.

Table 8 presents the three standard types of solutions that include the fragmentation time. The simplest, solution FD, leads to the separation of D on September 19, fails to fit the November 2 offset in right ascension by fully $2''$, and is therefore unacceptable. Solution FDT, although by far the best of the five in Table 8 in terms of fitting the two data points, is also unacceptable, because it implies the fragmentation time long before the activation of the nucleus. The FDN solution points to early September as the most likely fragmentation time,

Table 9. Residuals from fragmentation solutions for companion B of comet 168P.

Date 2012 (UT)	Observed offsets		Residuals “observed minus modeled” from solution ^a											
			FD		FDN		(DT) ₂		(DT) ₃		(DTN) ₁		(DTN) ₂	
			R.A.	Decl.	R.A.	Decl.	R.A.	Decl.	R.A.	Decl.	R.A.	Decl.	R.A.	Decl.
Oct. 26.42	-0 ^h .40	-2 ^m .06	-0 ^h .87	+0 ^m .40	-0 ^h .52	-0 ^h .05	-0 ^h .67	+0 ^h .19	-0 ^h .55	0 ^h .00	-0 ^h .60	-0 ^h .07	-0 ^h .51	-0 ^h .03
28.4	+0.30	-2.38	-0.25	+0.22	+0.03	-0.12	-0.08	+0.06	+0.03	-0.09	-0.03	-0.12	+0.05	-0.11
Nov. 2.3	+0.87	-2.77	+0.14	+0.18	+0.24	-0.11	+0.21	+0.16	+0.24	+0.12	+0.22	+0.13	+0.24	+0.11
2.44	+0.72	-3.22	-0.02	-0.26	+0.07	-0.32	+0.05	-0.28	+0.08	-0.32	+0.06	-0.31	+0.08	-0.32
3.28	+0.79	-3.00	+0.02	+0.02	+0.07	+0.01	+0.06	+0.02	+0.08	0.00	+0.07	+0.02	+0.08	0.00
6.28	+1.08	-3.12	+0.21	+0.09	+0.14	+0.26	+0.18	+0.19	+0.13	+0.24	+0.18	+0.26	+0.13	+0.25
6.30	+0.94	-3.47	+0.07	-0.26	0.00	-0.09	+0.04	-0.17	-0.01	-0.11	+0.04	-0.09	-0.01	-0.10
7.30	+1.09	-3.43	+0.18	-0.16	+0.07	+0.07	+0.12	-0.03	+0.05	+0.05	+0.13	+0.07	+0.06	+0.07
7.32	+0.87	-3.39	-0.03	-0.11	-0.15	+0.12	-0.09	+0.01	-0.17	+0.10	-0.09	+0.12	-0.16	+0.11

^a Fragmentation time adopted for a solution with subscript 1 is September 1.6 UT (onset time of outburst I), with subscript 2 is September 22.64 UT (onset of outburst II), and with subscript 3 is October 1.78 UT (onset of outburst III).

which is confirmed by even better fits based on solutions DT (Table 10) and DN, in which the coincidence was assumed between the fragmentation time and the onset time of outburst I. This outburst is likely to have accompanied the birth of companion D.

4.5. Companion E

Even though this companion was measured on four nights, it was possible to derive the fragmentation time only from solution FD (Table 8), but not from FDT or FDN, both of which failed to converge. This problem was the reason for abandoning, in the preliminary report (Sekanina 2012a), the scenario of companion E having been released from the primary and, instead, preferring it to be a fragment of companion B. With the present, much more extensive investigation, the offsets of E from what is now considered the best possible solution for B provide less attractive solutions to such a fragmentation scenario. While no solution for E relative to the primary offers an entirely satisfactory distribution of residuals, one has no choice but to accept as adequate solutions DT or DN, based on the assumption of this companion

having been released from the primary at the onset time of outburst I (Table 8). Both solutions yield rather similar residuals; the ones for solution DT are listed in Table 10. Identifying the fragmentation time with the onset time of outburst II or III leads to substantially inferior solutions, with the mean residuals near $\pm 0''.5$ or worse and with strongly systematic distributions of residuals.

4.6. Companion F

By contrast, the three measurements of this companion on two consecutive nights left little room for a broad variety of fragmentation scenarios. Solution FD, the only possible one that includes the fragmentation time as a variable, suggests rather unambiguously that this fragmentation event was related to outburst II (Table 8). Indeed, the table also shows three equivalent two-parameter solutions, DR, DT, and DN, which were obtained by forcing the fragmentation time to coincide with the onset time of this outburst. The residuals, acceptable under the circumstances, are in Table 10. No three- or four-parameter solutions could be made to converge.

4.7. Companion G

Only two images of this companion were measured on two consecutive nights, and the choice of fragmentation scenarios was as limited as in the case of companion F. Solution FD in Table 8 suggests that the birth of this companion was related to outburst I. When only the deceleration was solved for, the fit deteriorated a little, but equivalent two-parametric solutions in which the fragmentation time was forced to coincide with the onset time of outburst I had the same mean residual and the individual residuals virtually identical with those from solution FD (Table 10).

4.8. Summary of Findings on the Fragmentation Events

It is unfortunate that all six detected companions of this comet have been short-lived, none surviving for more than 11 weeks and mostly much less than that. The rather irritating experience with their appearance confirms that they all were typical cometary fragments in that they underwent dramatic brightness fluctuations with time, having been brighter than about magnitude 20 on only rather rare occasions. As a result, their observations were very scarce and their positional measurements exceedingly difficult.

Table 10. Residuals from some fragmentation solutions for companions C–G of comet 168P.

Companion	Date 2012 (UT)	Observed offsets		Residuals ^a from solutions			
				FD		DT ^b	
				R.A.	Decl.	R.A.	Decl.
C	Oct. 26.42	+2 ^h .45	-2 ^m .90	+0 ^h .17	-0 ^h .55	-0 ^h .29	-0 ^h .36
	Nov. 2.3	+4.60	-4.16	+0.28	+0.08	+0.25	-0.01
	2.44	+4.19	-4.01	-0.18	+0.27	-0.19	+0.17
	3.28	+4.78	-4.26	+0.13	+0.27	+0.19	+0.13
D	Nov. 2.3	+6.52	-9.35	+2.02	-0.69	+0.73	-0.34
	17.30	+6.75	-12.38	-0.65	+0.78	-0.62	+0.22
E	Nov. 2.44	+1.84	-4.86	+0.23	-0.13	+0.16	-0.09
	3.28	+2.42	-4.37	+0.75	+0.47	+0.69	+0.50
	7.31	+2.14	-5.61	+0.18	-0.26	+0.17	-0.28
	8.27	+1.57	-5.48	-0.45	-0.02	-0.45	-0.05
F	8.28	+1.45	-5.51	-0.58	-0.05	-0.57	-0.08
	Nov. 6.28	+4.78	-7.74	-0.20	-0.04	-0.20	-0.04
	6.30	+4.78	-7.98	-0.21	-0.27	-0.21	-0.27
G	7.31	+5.60	-7.68	+0.40	+0.31	+0.41	+0.31
	Nov. 11.35	+2.02	-9.49	-0.33	-0.10	-0.32	-0.11
	12.29	+2.71	-9.42	+0.32	+0.10	+0.32	+0.11

^a In the sense “observed minus modeled”.

^b Fragmentation times for these solutions are those adopted in Table 8.

Table 11. Adopted fragmentation solutions and relationships between outbursts and splitting of comet 168P.

Companion	Solution	Probably Differential Separation			Endurance (equiv. days)
		related outburst ^a	deceleration (units ^b)	velocity ^c (m/s)	
B	DTN	II	17.1	0.16	22.3
C	DT	III	49.5	0.12	15.9
D	DN	I	12.0	0.53	37.1
E	DT	I	9.2	0.05	33.0
F	DT	II	36.9	0.03	22.3
G	DT	I	14.1	0.04	34.8

^a Its onset time (Table 6) determines the adopted time of separation of the companion from the primary.

^b Units are 10^{-5} the solar gravitational acceleration, or $0.059 \mu\text{m/s}^2$ at 1 AU from the Sun.

^c This is the total magnitude of the separation velocity; for its components, see column “Solution” and Table 8.

It is highly probable that all six companions separated directly from the primary. The fragmentation solutions offered in Table 8 show, however, that because of the scarcity of observations it was never possible to solve for all five parameters or even four parameters of the fragmentation model. One of the corollaries of this problem is a greater than expected error in the fragmentation times derived. This is true for all six fragments, including B, the best observed one. Under these circumstances, one cannot expect to *prove* that the times of the fragmentation events truly coincided with the onset times of the outbursts. Rather, one needs to take it for granted that for comet 168P the two categories of phenomena *were* closely related and, on this assumption, try to figure out which outburst might have accompanied each of the fragmentation episodes.

This objective was for each companion discussed in the preceding subsections. The adopted fragmentation solutions and the relationships between the outbursts and the fragmentation events are summarized in Table 11. The most likely scenario that emerges from this table is that outburst I coincided with the separation of three companions, while outburst II accompanied the birth of two companions and outburst III just one companion. The relationships between outburst I and companion G, between outburst II and companion F, and between outburst III and companion C are proposed with somewhat greater confidence than the relationships between outburst I and companions D and E, and between outburst II and companion B.

These assignments, if correct, are remarkable in that the least powerful explosion event of the three, outburst I (Sec. 3.2), correlates with three companions, while the most powerful one, outburst II, with only two companions. Thus, the amount of ejected dust appears to be inversely correlated with the mass released intact at least when comparing outbursts I against II and I against III. This could mean that the total mass of the lost solid material may not have varied dramatically from event to event, but its overall mechanical strength may have.

The last column of Table 11 presents the observed endurance E of the companions, defined (Sekanina 1977, 1982) as the interval of time, $t_{\text{frag}} - t_{\text{last}}$, between fragmentation and the last observation, weighted by an inverse square power law of heliocentric distance r , thereby measuring each fragment’s minimum lifetime against its

outgassing, whose rate is approximated by the r^{-2} law. Thus,

$$E = \int_{t_{\text{frag}}}^{t_{\text{last}}} \frac{dt}{r^2} = 1.015 p^{-\frac{1}{2}} (u_{\text{last}} - u_{\text{frag}}), \quad (5)$$

where p is the semilatus rectum of the fragment’s orbit (which for all fragments of 168P can be approximated by the value of p of the comet’s orbit) and u_{last} and u_{frag} are the true anomalies at the times of, respectively, the last observation and fragmentation. When p is in AU and the true anomalies in degrees, the endurance is expressed in equivalent days, that is, the days at 1 AU from the Sun.

The plot of the endurance E of 24 companions of 18 split comets against their differential deceleration γ shows (Sekanina 1982) that E generally increases with decreasing γ and that this relationship is described by

$$E = \Lambda \gamma^{-0.4}, \quad (6)$$

where Λ is a constant and γ is in units of 10^{-5} the solar gravitational acceleration. A great majority of fragments of the split comets follows this empirical law with $\Lambda = 200$ equivalent days. However, a small group of sturdier, relatively massive objects ($\gamma < 10$ units) satisfies law (6) with $\Lambda \simeq 800$ equivalent days, while another group of five very brittle, low-mass fragments, whose $\gamma > 60$ units, fits law (6) with $\Lambda = 87$ equivalent days. The surprising finding from Table 11 is that all six companions of comet 168P match closely an extrapolated $E(\gamma)$ relationship of this group of very brittle fragments, as seen from Figure 3.

The five fragments in this group that broke off from earlier comets are, in the order of decreasing γ , companion C to C/1899 E1 (Swift) and companions B to C/1906 E1 (Kopff), C/1942 X1 (Whipple-Fedtko-Tevezadze), C/1968 U1 (Wild), and C/1969 T1 (Tago-Sato-Kosaka). The first two are Oort-cloud comets, while C/1969 T1 and C/1942 X1 have the original orbital periods of about 90,000 years and 1600 years, respectively. The orbit of comet C/1968 U1 has not been determined to adequate accuracy to establish its origin. In any case, 168P is the first short-period comet whose companions belong to this group of excessively brittle fragments.

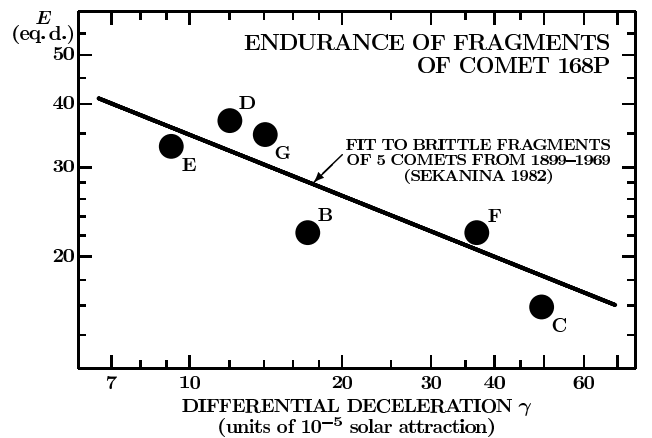


Figure 3. Endurance of the companions of comet 168P as a function of their differential deceleration due to outgassing. The straight line is not a fit to the plotted data points, but extrapolated from that to very brittle fragments of five comets from 1899–1969.

One may further add that this excessive brittleness explains not only the unusually short lifetimes of the companions of 168P, but it also fits the observers' reports that the companions displayed generally a tendency toward progressive elongation, a sign that they already consisted of expanding clusters of subfragments subjected to a range of decelerations. This accelerating disintegration of subfragments into boulders, pebbles, and coarse dust is a characteristic property of the advanced phase of the process of cascading fragmentation and has recently been under different circumstances demonstrated by comet C/2011 W3 only days after its passage through the Sun's inner corona (Sekanina and Chodas 2012).

Thanks to comet 168P, the global picture of the plot of the endurance E versus the deceleration γ changes in the sense that the previous range of decelerations in this group of excessively brittle fragments, between 65 and 480 units of 10^{-5} the solar gravitational acceleration, is now greatly extended beyond the lower limit of γ all the way to slightly less than 10 units, that is, the range in $\log \gamma$ has nearly doubled, showing that this group is by no means limited to merely dwarf fragments.

It is noticed that some results in my first preliminary report on the fragmentation sequence (Sekanina 2012a) differed from these final conclusions. The differences are due in part to the data point on the companion D until recently unavailable, in part to a more comprehensive analysis now undertaken. The results of the second preliminary report (Sekanina 2012b) have now been closely confirmed.

5. MASS OF MATERIAL TRAILING THE NUCLEUS OF 168P

Hergenrother (2012a) called attention to a mass of material appearing, in numerous images taken in the second half of October, to move away from the near-nuclear region in the antisolar direction. First detected in the high-resolution images exposed with the Faulkes-North 200-cm reflector on October 16, the feature was present until at least October 23, but the Faulkes images from October 26 no longer show it. On the very likely premise — supported by the fairly high values of $Af\rho$ in this period of time (Sec. 3.2) — that this mass consisted of dust ejecta, its position angles measured by Hergenrother are compared in Table 12 with the position angles computed for the best-fitting synchronic formation. The corresponding most probable time of the emitted material is October 5.8 ± 0.6 UT. However, it was pointed out by Sostero et al. in their blog¹² that the images acquired with the Faulkes-North telescope on October 22.44 UT showed this “diffuse trail” to be about 6'' long and 3'' wide, the width suggesting that the duration of the emission event was nontrivial, extending perhaps over a period of a few days or so. The overall timing of this feature's emission appears unquestionably to be related to outburst III and the release of companion C. The positional correlation between the mass of trailing material and companion C was noticed by Hergenrother (2012a), and the suspicion that this mass was a product of outburst III was expressed by the author in the same communication note (Sekanina 2012a).

¹² The blog, dated October 22, 2012, by G. Sostero, N. Howes, A. Tripp, and E. Guido, <http://remanzacco.blogspot.it/2012/10/update-on-comet-168phergenrother.html>.

The dimensions of dust particles in this trailing mass can be estimated from the length of the synchronic feature. Its just mentioned extension on October 22.44 suggests that the dust was subjected to a maximum solar radiation-pressure acceleration of ~ 0.0018 the Sun's gravitational acceleration, which at an assumed bulk density of 0.4 g/cm^3 is equivalent to a minimum particle diameter of $\sim 1.6 \text{ mm}$. Thus, the observed mass was made up of dust mostly in the millimeter-centimeter size range. Curiously and perhaps not quite coincidentally, this limiting particle diameter is identical to that derived for the dust population situated at the tip of the spine tail of comet C/2011 W3 after it lost its nuclear condensation (Sekanina and Chodas 2012).

6. CONCLUSIONS

Comets are notorious for always changing their brightness, but not every brightening is called an outburst. To belong to this category of events, a brightness surge must satisfy three critical conditions: it must be sudden, sufficiently prominent (amplitude of at least 0.8–1.0 magnitude), and unexpected. Countless studies have shown that the total amount of material ejected from the nucleus during an outburst is always less (usually far less) than 10^{13} grams and that an outburst produces a *local* event on the scale of the dimensions of an average comet nucleus. Outbursts differ from the very rare giant explosions, which are much more massive and powerful. During the outbursts, to which some comets are more prone than other, both dust and gas are released from the nucleus, but there is a wide range of these events in terms of the dust-to-gas mass ratio. It is therefore appropriate to talk about dust-dominated and gas-dominated outbursts. Their differences are revealed not only spectroscopically, but also by their unequal temporal profiles, as the history of their observations clearly documents.

Because a major attribute of outbursts is a steep light surge in the initial stage of a “stellar nucleus” — an unresolved image of an expanding plume of ejected material — a fundamental parameter of these events is their onset time. An extra dimension to this parameter is provided by the fact that outbursts often coincide with the comets' fragmentation events, and the onset time can be used to correlate the two classes of phenomena. In the absence of accurate information on the timing of a fragmentation event, an outburst's onset time can even be used as a proxy for the separation time of a nuclear fragment. In the case of multiple outbursts and multiple fragmentation of a comet, this approach can be applied to test various fragmentation/outburst sequences and scenarios. This is the case of comet 168P/Hergenrother.

Table 12. Comparison of measured and computed position angles of the mass of material and the position angle of the prolonged radius vector of comet 168P.

Time of observation 2012 UT	Position angle of mass of material			Position angle of radius vector
	measured	computed	o-c ^a	
Oct. 16.45	142°	142°.1	−0°.1	127°.5
20.25	140	140.4	−0.4	122.2
21.35	141	140.0	+1.0	120.9
22.44	139	139.6	−0.6	119.5

^a Residual “observed minus computed”

Next I show that the so-called nuclear magnitudes, published in the MPCs and the MPECs for comets that are observed by means of CCD arrays primarily for astrometric purposes, can despite their poor reputation be used to great advantage in an effort to tightly constrain the onset time of outbursts in objects that are extensively monitored. Although it is inadmissible to mix the nuclear magnitudes reported for the same comet by different observers without first carefully examining their possible compatibility, it is legitimate to combine the temporal constraints on an outburst's onset time derived from timing of images reported by the various observers, as long as the conditions derived from this timing independently and consistently confirm the overall outcome and, if so happens, any minor inconsistencies are fully understood in terms of the observational setups.

Extensive application of the developed technique to comet 168P shows that the object underwent three separate outbursts during a one-month period between the beginning of September and the beginning of October 2012. Toward the end of October, yet another modest surge of activity occurred, but it was neither sudden nor prominent enough to be classified as an outburst. Afterwards, the comet's activity was steadily decreasing with no flare-ups worth mentioning, the monitoring having been terminated before mid-December, 70 days post perihelion. The amplitudes of the three outbursts were used to estimate their peak rates of brightness surge in arbitrary intensity units; their ratio was found to be 2:20:15.

High-resolution imaging of comet 168P revealed the existence of six companion nuclei, B–G, to the primary A between October 26 and November 17. The modeling of their motions suggested that they all broke off from the primary and that the comet was indeed fragmenting profusely during the period of time covered by the three outbursts. Whereas the exact fragmentation times could not be established from the limited astrometric data, closer examination suggested that the first outburst was most likely to accompany the release of companions D, E, and G; the second outburst to be associated with the birth of B and F; and the last outburst to coincide with the separation of C. The peak rates of brightness surge do not at all appear to be correlated with the number of fragments released. This tendency to an anticorrelation between fragmentation and the magnitude of outbursts could mean that the material losses during the three outbursts were comparable in mass, but that most of the mass separated in the first outburst remained fairly intact during the liftoff, while most of the mass lost in the last outburst disintegrated into dust very soon. This scenario is supported by the detection of a cloud of material, found to have been ejected in early October, at a time that closely correlates with the time of the last outburst and the birth of companion C. All six companions belong to a group of very brittle fragments, which explains their short lifetimes and elongated shape.

I thank Carl W. Hergenrother for his unpublished measurement of the position of a suspected companion — that turned out to be fragment D — in the images of comet 168P he took with the VATT reflector on November 17. I also thank him for reading and commenting on the manuscript of this paper. Finally, I thank Dr. Daniel W. E. Green for his editorial work. This research

was carried out at the Jet Propulsion Laboratory, California Institute of Technology, under contract with the National Aeronautics and Space Administration.

REFERENCES

- Abetti, A. (1883). Osservazioni della cometa Pons-Brooks, *Astron. Nachr.* **107**, 223–228.
- A'Hearn, M. F.; D. G. Schleicher; P. D. Feldman; R. L. Millis; and D. T. Thompson (1984). Comet Bowell 1980b, *Astron. J.* **89**, 579–591.
- A'Hearn, M. F.; R. L. Millis; D. G. Schleicher; D. J. Osip; and P. V. Birch (1995). The ensemble properties of comets: Results from narrowband photometry of 85 comets, 1976–1992, *Icarus* **118**, 223–270.
- Beyer, M. (1962). Physische Beobachtungen von Kometen. XII, *Astron. Nachr.* **286**, 219–240.
- Bobrovnikoff, N. T. (1931). Halley's Comet in its apparition of 1909–1911, *Publ. Lick Obs.* **17**, 305–482.
- Bobrovnikoff, N. T. (1932). On the phenomena of halos in comets, *Publ. Astron. Soc. Pacific* **44**, 296–307.
- Bobrovnikoff, N. T. (1943). The Periodic Comet Holmes (1892 III), *Pop. Astron.* **51**, 542–551.
- Campbell, W. W. (1893). The spectrum of Holmes' Comet, *Publ. Astron. Soc. Pacific* **5**, 99–100.
- Chandler, S. C., Jr. (1883). On the outburst in the light of the comet Pons-Brooks Sept. 21–23, *Astron. Nachr.* **107**, 131–134.
- Crovisier, J., D. Bockelée-Morvan; E. Gérard; H. Rauer; N. Biver; P. Colom; and L. Jorda (1996). What happened to comet 73P/Schwassmann-Wachmann 3?, *Astron. Astrophys.* **310**, L17–L20.
- Gonzalez, J. J. (2012). Comet 168P/Hergenrother, *Centr. Bureau Electr. Tel.* 3257.
- Green, D. W. E., ed. (1995). Comet 41P/Tuttle-Giacobini-Kresák, *IAU Circ.* 6207.
- Green, D. W. E., ed. (1997a). Astrometry of comets, in *The ICQ Guide to Observing Comets*, Smithsonian Astrophysical Observatory, Cambridge, Mass., pp. 151–157.
- Green, D. W. E., ed. (1997b). CCD observations, in *The ICQ Guide to Observing Comets*, Smithsonian Astrophysical Observatory, Cambridge, Mass., pp. 94–104.
- Green, D. W. E., ed. (2012). Comet 168P/Hergenrother, *Centr. Bureau Electr. Tel.* 3257.
- Hergenrother, C. W. (2012a). Comet 168P/Hergenrother, *Centr. Bureau Electr. Tel.* 3295.
- Hergenrother, C. W. (2012b). Comet 168P/Hergenrother, *Centr. Bureau Electr. Tel.* 3318.
- Herschel, J. F. W. (1847). *Results of Astronomical Observations Made During the Years 1834, 5, 6, 7, 8, at the Cape of Good Hope*, Chapter V, pp. 393–413. Smith, Elder & Co., Cornhill. London, U.K.
- Jehin, E.; H. Boehnhardt; Z. Sekanina; X. Bonfils; O. Schütz; J.-L. Beuzit; M. Billeres; G. J. Garrard; P. Leisy; and F. Marchis (2002). Split comet C/2001 A2 (LINEAR), *Earth Moon Plan.* **90**, 147–151.
- Jewitt, D. (1990). The persistent coma of Comet P/Schwassmann-Wachmann 1, *Astrophys. J.* **351**, 277–286.
- Kammermann, A. (1893). Beobachtungen des Cometen 1892 III (Holmes), *Astron. Nachr.* **132**, 61–62.
- Kidger, M. R. (2002). Spanish monitoring of comets: Making sense of amateur photometric data, *Earth Moon Plan.* **90**, 259–268.
- Kresák, L'. (1974). The outbursts of periodic comet Tuttle-Giacobini-Kresák, *Bull. Astron. Inst. Czech.* **25**, 293–304.
- Li, J.; D. Jewitt; J. M. Clover; and B. V. Jackson (2011). Outburst of Comet 17P/Holmes observed with the Solar Mass Ejection Imager, *Astrophys. J.* **728**, 31–39.
- Meech, K. J.; M. J. S. Belton; B. E. A. Mueller; M. W. Dickson; and H. R. Li (1993). Nucleus properties of P/Schwassmann-Wachmann 1. *Astron. J.* **106**, 1222–1236.
- Moreno, F. (2009). The dust environment of Comet 29P/Schwassmann-Wachmann 1 from dust tail modeling of 2004 near-perihelion observations, *Astrophys. J. Suppl. Ser.* **183**, 33–45.
- Müller, G. (1884a). Über einen zweiten merkwürdigen Lichtausbruch an dem Cometen Pons-Brooks 1884 Jan. 1, *Astron. Nachr.* **107**, 381–384.

- Müller, G. (1884b). Photometrische Beobachtungen des Cometen Pons-Brooks, *Astron. Nachr.* **108**, 161–170.
- Palisa, J. (1893). Ueber eine plötzliche Aenderung im Aussehen des Cometen 1892 III (Holmes), *Astron. Nachr.* **132**, 15–16, 31–32.
- Pickering, E. C.; A. Searle; and O. C. Wendell (1900). Observations of comets, *Ann. Harv. Coll. Obs.* **33**, 149–158.
- Schiaparelli, G. V. (1883). Osservazioni della cometa Pons-Brooks, *Astron. Nachr.* **107**, 139–144.
- Schleicher, D. G. (2012). Comet 168P/Hergenrother, *Centr. Bureau Electr. Tel.* 3257.
- Schlosser, W.; R. Schulz; and P. Koczet (1986). The cyan shells of comet P/Halley, in *Exploration of Halley's Comet*, Proc. 20th ESLAB Symp., ESA SP-250, B. Battrock, E. J. Rolfe, and R. Reinhard, eds., ESTEC, Noordwijk, vol. 3, pp. 495–498.
- Schulz, R., and W. Schlosser (1990). CN jets as progenitors of CN shells in the coma of Comet P/Halley, in *Formation of Stars and Planets, and the Evolution of the Solar System*, ESA SP-315, B. Battrock, ed., ESTEC, Noordwijk, pp. 121–125.
- Sekanina, Z. (1977). Relative motions of fragments of the split comets. I. A new approach, *Icarus* **30**, 574–594.
- Sekanina, Z. (1978). Relative motions of fragments of the split comets. II. Separation velocities and differential decelerations for extensively observed comets, *Icarus* **33**, 173–185.
- Sekanina, Z. (1982). The problem of split comets in review, in *Comets*, L. L. Wilkening, ed., University of Arizona, Tucson, pp. 251–287.
- Sekanina, Z. (1990). Gas and dust emission from comets and life spans of active areas on their rotating nuclei, *Astron. J.* **100**, 1293–1314, 1389–1391.
- Sekanina, Z. (1993). Computer simulation of the evolution of dust coma morphology in an outburst: P/Schwassmann-Wachmann 1, in *On the Activity of Distant Comets*, W. F. Huebner, H. U. Keller, D. Jewitt, J. Klinger, and R. West, eds., Southwest Research Institute, San Antonio, TX, pp. 166–181.
- Sekanina, Z. (2005). Comet 73P/Schwassmann-Wachmann: Nucleus fragmentation, its light-curve signature, and close approach to earth in 2006, *Int. Comet Quart.* **27**, 225–240.
- Sekanina, Z. (2008a). Exploding comet 17P/Holmes, *Int. Comet Quart.* **30**, 3–28.
- Sekanina, Z. (2008b). On a forgotten 1836 explosion from Halley's comet, reminiscent of 17P/Holmes' outbursts, *Int. Comet Quart.* **30**, 63–74.
- Sekanina, Z. (2012a). Comet 168P/Hergenrother, *Centr. Bureau Electr. Tel.* 3295.
- Sekanina, Z. (2012b). Comet 168P/Hergenrother, *Centr. Bureau Electr. Tel.* 3318.
- Sekanina, Z.; and P. W. Chodas (2002). Common origin of two major sungrazing comets, *Astrophys. J.* **581**, 760–769.
- Sekanina, Z., and P. W. Chodas (2012). Comet C/2011 W3 (Lovejoy): Orbit determination, outbursts, disintegration of nucleus, dust-tail morphology, and relationship to new cluster of bright sungrazers, *Astrophys. J.* **757**, 127 (33pp).
- Sekanina, Z.; E. Jehin; H. Boehnhardt; X. Bonfils; O. Schuetz; and D. Thomas (2002). Recurring outbursts and nuclear fragmentation of comet C/2001 A2 (LINEAR), *Astrophys. J.* **572**, 679–684.
- Sostero, G.; N. Howes; A. Tripp; P. Phelps; and E. Guido (2012). Comet 168P/Hergenrother, *Centr. Bureau Electr. Tel.* 3295.
- Spahr, T. B.; G. V. Williams; S. Nakano; and A. Doppler, eds. (2012). Comet 168P/Hergenrother, *Minor Planet Circ.* 80422–80429.
- Stansberry, J. A.; J. Van Cleve; W. T. Reach; D. P. Cruikshank; J. P. Enery; Y. R. Fernandez; V. S. Meadows; K. Y. L. Su; K. Misselt; G. H. Rieke; E. T. Young; M. W. Werner; C. W. Engelbracht; K. D. Gordon; D. C. Hines; D. M. Kelly; J. E. Morrison; and J. Muzerolle (2004). Spitzer observations of the dust coma and nucleus of 29P/Schwassmann-Wachmann 1, *Astrophys. J. Suppl. Ser.* **154**, 463–468.
- Stevenson, R. A.; J. M. Bauer; J. R. Masiero; and A. K. Mainzer (2012). Comet 168P/Hergenrother, *Centr. Bureau Electr. Tel.* 3295.
- Struve, H. (1884). Beobachtungen des Cometen 1884 I (Pons 1812) am 15 zöll. Refractor in Pulkowa, *Astron. Nachr.* **109**, 369–386.
- Swings, J.-P.; and J.-M. Vreux (1973). Observations spectrographiques de la comète 1973b immédiatement après son violent sursaut de brillance de juillet 1973, *Bull. Soc. Roy. Sci. Liège* **42**, 593–597.
- Trigo-Rodríguez, J. M.; E. Garcia-Melendo; B. J. R. Davidsson; A. Sánchez; D. Rodríguez; J. Lacruz; J. A. De los Reyes; and S. Pastor (2008). Outburst activity in comets. I, *Astron. Astrophys.* **485**, 599–606.
- Trigo-Rodríguez, J. M.; D. A. Garcia-Hernández; A. Sánchez; J. Lacruz; B. J. R. Davidsson; D. Rodríguez; S. Pastor; and J. A. de los Reyes (2010). Outburst activity in comets. II, *Mon. Not. Roy. Astron. Soc.* **409**, 1682–1690.
- Vogel, H. C. (1884). Einige Beobachtungen über den Cometen Pons-Brooks, insbesondere über das Spectrum desselben, *Astron. Nachr.* **108**, 21–26.
- Vogel, H. C. (1893). Ueber das Spectrum des Cometen 1892 III (Holmes), *Astron. Nachr.* **131**, 373–374.
- Whipple, F. L. (1980). Rotation and outbursts of comet P/Schwassmann-Wachmann 1, *Astron. J.* **85**, 305–313.